

High cycle compressive fatigue of unidirectional glass/polyester performed at high frequency
by Andrew Jay Belinky

A thesis submitted in partial fulfillment of the requirements for the degree of Master of Science in Chemical Engineering
Montana State University
© Copyright by Andrew Jay Belinky (1994)

Abstract:
This thesis is part of current materials research aimed at studying the behavior of polymer matrix composites at high cycles. The need stems from wind turbines which experience roughly 10^8 to 10^9 fatigue cycles (application and relaxation of load) during their 20 to 30 year lifetimes. Conventional fatigue testing is limited to 20 Hz (cycles per second) because of hysteresis heating problems caused by poor heat transfer capabilities of polymer matrix composites. However, at 20 Hz it would take 58 days to almost 1.5 years to reach the desired 10^8-10^9 cycle range. Previous work by Creed [3] demonstrated that high frequency (75 to 100 Hz) tensile fatigue testing can be accomplished using a specimen that is sufficiently thin that hysteretic heating is no longer a problem. The purposes of this research were to develop a high frequency compressive fatigue test method and obtain base line fatigue data for unidirectional glass/ polyester composites at R values (minimum stress/ maximum stress) of ten and two.

Two-ply specimens were cut from composite plates manufactured by resin transfer molding (RTM). Specimen geometry measured 2.2 inches long by 0.25 inches wide by approximately 0.035 inches thick. Fiber volume fraction was found to vary between the composite plate and individual specimens depending on the number of fiber bundles present in an individual specimen; however, no significant effects. of fiber content were observed in the S/N (stress versus number of cycles to failure) curves. Specimen porosity ranged from 2% to 4%.

S/N data and specimen failure modes for R=10 were in good agreement with literature data and with data from standard sized coupons manufactured from the same material as the high frequency specimens but tested at lower frequencies (10-20 Hz). The data approximately followed an 8% per decade decay line. For R=2 the data approximately followed a least squares 5.5% per decade decay line. Above 10^5 cycles the S/N curves for R=10 and R=2 flattened, and least square curve fits of these points (including runouts) showed that projected failure stresses at 10^9 cycles rose for both curves compared to curve fits using the entire data set. Frequency effects were examined using high frequency specimens tested at various frequencies but the same stress level. Data at 30 and 50 Hz correlated well, but some specimens at 10 Hz had longer lifetimes.

HIGH CYCLE COMPRESSIVE FATIGUE OF UNIDIRECTIONAL GLASS/POLYESTER PERFORMED AT HIGH FREQUENCY

by

Andrew Jay Belinky

A thesis submitted in partial fulfillment
of the requirements for the degree

of

Master of Science

in

Chemical Engineering

MONTANA STATE UNIVERSITY
Bozeman, Montana

April 1994

N378
B4124

APPROVAL

of a thesis submitted by

Andrew Jay Belinky

This thesis has been read by each member of the thesis committee and has been found to be satisfactory regarding content, English usage, format, citations, bibliographic style, and consistency, and is ready for submission to the College of Graduate Studies.

4/25/94 — Date

John D Mandell — Chairperson, Graduate Committee

Approved for the Major Department

Apr 25, 1994 — Date

John A Sears — Head, Major Department

Approved for the College of Graduate Studies

5/3/94 — Date

R L Brown — Graduate Dean

STATEMENT OF PERMISSION TO USE

In presenting this thesis in partial fulfillment of the requirements for a master's degree at Montana State University, I agree that the Library shall make it available to borrowers under rules of the Library.

If I have indicated my intention to copyright this thesis by including a copyright notice page, copying is allowable only for scholarly purposes, consistent with "fair use" as prescribed in the U.S. Copyright Law. Requests for permission for extended quotation from or reproduction of this thesis in whole or in parts may be granted only by the copyright holder.

Signature Andrew J. Belinky

Date 4/25/94

ACKNOWLEDGMENTS

In the course of the past two years, numerous individuals were instrumental in assisting with this research. First and foremost, I would like to thank Dr. John Mandell for his guidance and suggestions which have made this learning process very valuable. Jane Curtis and Monica Hoey helped with purchasing materials and navigated me through administrative waters. Lyman Fellows was instrumental in turning my designs into reality in the lab. Neil Wahl assisted in the signal analysis. Chuck Hedley, Dan Samborsky, and Dave Combs provided endless hours of conversation and idea swapping which kept me sain and provided solutions to some pressing research problems.

Finally, I would also like to thank Sandia National Laboratories (Contract No. 40-8875) for its support of this research and the wind turbine energy project.

TABLE OF CONTENTS

1. INTRODUCTION 1

2. BACKGROUND 4
   - General Fatigue Properties 4
   - Compression Dominated Fatigue 10
   - Compression Test Methods 14
   - Frequency Effects 18

3. EXPERIMENTAL METHODS 23
   - Mechanical Testing Equipment 23
   - Specimen Fabrication 25
   - Porosity Measurement 29
   - Fiber Content Measurement 32
   - Fracture Surface Examination 33

4. RESULTS AND DISCUSSION 34
   - Test Development 34
     - Compression 34
     - Tensile Fatigue 41
   - Fatigue Results 44
     - Compression 45
     - Effect of Fiber Content Variations on S/N Curves 56
     - Tension 60
   - Failure Modes 68
   - Frequency Effects 74

5. CONCLUSIONS AND RECOMMENDATIONS 82
   - Conclusions 82
   - Recommendations for Further Research 85

REFERENCES 89

APPENDIX - GRIP DESIGN 94

LIST OF TABLES

Table Page

1. Data for R=10 S/N Curve. 47
2. Data for R=2 S/N Curve. 53
3. Fiber Volume Fraction Data for R=10 Curve. 58
4. Fiber Volume Fraction Data for R=2 Curve. 60
5. Data for R=0.1 S/N Curve. 63
6. Frequency Effects (R=10). 75

LIST OF FIGURES

Figure		Page
1.	Damage Modes During Fatigue Life [4].	10
2.	Model of Compressive Failure Modes [15].	11
3.	Composite Compression Failure Modes [16].	12
4.	Instron 8511 Servohydraulic Test Machine.	23
5.	Hexcel Unidirectional E-glass Cloth No. 0155-50.	26
6.	RTM Setup.	28
7.	Fiber Bundle Arrangement in Specimen.	30
8.	Fiber Bundle Arrangement at Specimen Edge.	30
9.	Fiber and Pore Arrangement in Fiber Bundle.	31
10.	Fiber and Pore Arrangement in Fiber Bundle.	31
11.	Failure Mode for Early Specimens with Four Plies of Roving.	36
12.	Failure Mode for Three Plies of Unidirectional Cloth.	37
13.	Compression Specimen Geometry.	38
14.	Fatigue Data Illustrating the Effect of Misaligned Specimens.	40
15.	Compressive Stress-Strain Curve of Glass/ Polyester.	41
16.	Tensile Specimen Geometry.	43

17. Tensile Stress-Strain Curve for Unidirectional Glass/ Polyester. 44
18. Sine waves for R Values of 10, 2, and 0.1. 45
19. High Frequency S/N Data for R=10. 48
20. Comparison of Small Specimen High Frequency S/N Data with Standard Coupon Low Frequency Data. . . 49
21. High Frequency S/N Data for R=10 Above 10^5 Cycles. 51
22. High Frequency S/N Data for R=2. 54
23. Comparison of R=10 and R=2 S/N Data. 55
24. High Frequency Data for R=2 Above 10^5 Cycles. . . 57
25. Possible Packing Arrangements for Fiber Bundles. . 59
26. Comparison of R=10 S/N Curve with Specimen Fiber Volume Fraction Taken into Account and Ignored (power law fit is to data not normalized by fiber content). 61
27. Comparison of R=2 S/N Curve with Specimen Fiber Volume Fraction Taken into Account and Ignored (power law fit is to data not normalized by fiber content). 62
28. High Frequency S/N Data for R=0.1. 64
29. High Frequency S/N Data for R=0.1 Above 10^5 Cycles. 65
30. Comparison of High Frequency R=0.1 Data from Creed [3] and This Research. 66
31. Failure Modes Observed by Combs [39]. 68
32. Failure Modes Observed by Conners et. al. [35]. . 69

33. Failure Mode of Inner Plies of Specimens Used by Combs [39]. 69
34. Failure Modes Observed in this Research. 70
35. Edge View of Failure Zone. 71
36. Angled View of Failure Zone. 71
37. Fracture Surface of Static Specimen (AC14). . . . 72
38. Low Stress Fatigue Fracture Surface (AC15). . . . 72
39. High Stress Fatigue Fracture Surface (AC8). . . . 73
40. Unfiltered Load Feedback Waveforms for 10 and 100 Hz. 76
41. Signal Amplitude versus Frequency for 10 Hz. . . . 78
42. Signal Amplitude versus Frequency for 100 Hz. . . 79
43. Filtered Load Feedback Waveforms for 10 and 100 Hz. 80
44. Grips Used in Previous Research by Creed. 95
45. Grips Used in This Research with Specimen Running. 96
46. Diagram of Grips. 97

ABSTRACT

This thesis is part of current materials research aimed at studying the behavior of polymer matrix composites at high cycles. The need stems from wind turbines which experience roughly 10^8 to 10^9 fatigue cycles (application and relaxation of load) during their 20 to 30 year lifetimes. Conventional fatigue testing is limited to 20 Hz (cycles per second) because of hysteresis heating problems caused by poor heat transfer capabilities of polymer matrix composites. However, at 20 Hz it would take 58 days to almost 1.5 years to reach the desired 10^8-10^9 cycle range. Previous work by Creed [3] demonstrated that high frequency (75 to 100 Hz) tensile fatigue testing can be accomplished using a specimen that is sufficiently thin that hysteretic heating is no longer a problem. The purposes of this research were to develop a high frequency compressive fatigue test method and obtain base line fatigue data for unidirectional glass/ polyester composites at R values (minimum stress/ maximum stress) of ten and two.

Two-ply specimens were cut from composite plates manufactured by resin transfer molding (RTM). Specimen geometry measured 2.2 inches long by 0.25 inches wide by approximately 0.035 inches thick. Fiber volume fraction was found to vary between the composite plate and individual specimens depending on the number of fiber bundles present in an individual specimen; however, no significant effects of fiber content were observed in the S/N (stress versus number of cycles to failure) curves. Specimen porosity ranged from 2% to 4%.

S/N data and specimen failure modes for R=10 were in good agreement with literature data and with data from standard sized coupons manufactured from the same material as the high frequency specimens but tested at lower frequencies (10-20 Hz). The data approximately followed an 8% per decade decay line. For R=2 the data approximately followed a least squares 5.5% per decade decay line. Above 10^5 cycles the S/N curves for R=10 and R=2 flattened, and least square curve fits of these points (including runouts) showed that projected failure stresses at 10^9 cycles rose for both curves compared to curve fits using the entire data set. Frequency effects were examined using high frequency specimens tested at various frequencies but the same stress level. Data at 30 and 50 Hz correlated well, but some specimens at 10 Hz had longer lifetimes.

CHAPTER ONE

INTRODUCTION

Within the past 30 years composite materials have made their way into a variety of structural components. From aircraft to automobiles, the desire to reduce weight while maintaining or increasing strength and stiffness has led engineers to turn to composites. This is nowhere more evident than in the newly resurgent wind energy industry. Based on the wooden windmills used by farmers to pump water for decades, the new wind power turbines are designed to be inexpensive, light weight, efficient, and produce electricity for communities at a rate competitive with current gas and possibly coal facilities. To achieve these objectives, manufacturers chose E-glass/ polyester or vinylester composites for their turbine blades. A dearth of information on material fatigue properties and blade service loading, as well as design and fabrication flaws, resulted in poor early machines that often failed far short of their projected 20 to 30 year life.

It is now known that wind disruption by the generator tower causes the turbine blade loads to change significantly each time they pass the structure (one per revolution). Each bending constitutes a major fatigue cycle where the blade

experiences a loading and unloading of the applied wind load. Given that turbines rotate at one to three revolutions per second, a blade can experience between 10^8 and 10^9 fatigue cycles in its proposed 20 to 30 year lifetime [1]. Turbulence and other factors can also excite other vibration modes in the blades, causing higher frequency but usually lower amplitude fatigue cycles [2].

Presently, fatigue data for blade materials out to the high cycle range are very scarce, due mainly to the limited speed at which conventional fatigue tests can be performed. For E-glass/ polyester, 20 Hz (cycles per second) is a typical upper frequency limit; above this, internal heating becomes a major concern, and thermal failure can actually precede mechanical failure. At 20 Hz, though, a test to 10^8 cycles would last 58 days, and to reach 10^9 cycles would require almost one and a half years [1]. This is very important since it would take many years to characterize the fatigue behavior of a single material, and complications with testing equipment such as breakdowns and power outages would make successful long term tests very difficult to complete. The only alternative has been to extrapolate lower cycle data to high cycles, with no confidence in the extrapolation procedure. Therefore, current materials research is aimed at developing high frequency test methods which allow fatigue data to be obtained out to the 10^8-10^9 region in a reasonable amount of time. The basis for high frequency tests is to minimize test

specimen thickness in order to improve heat transfer while maintaining the basic failure mode of larger specimens.

This thesis is a part of the overall materials testing program. Previous work focused on tensile fatigue and designing a test method to run longitudinal unidirectional specimens at high frequencies (75 to 100 Hz) [3]. The present study extends this work to longitudinal compression fatigue at high frequencies (75 to 100 Hz).

CHAPTER TWO

BACKGROUND

General Fatigue Properties

The fatigue behavior of fiber composites varies greatly compared with that of homogeneous materials. This is due primarily to the high degree of heterogeneity and anisotropy in composites. In isotropic materials such as metals, most of the fatigue life is spent nucleating and growing a single dominant crack. When the crack reaches a critical size, catastrophic failure results. With fiber-reinforced composites, however, damage often occurs on the very first cycle and there are numerous failure modes such as matrix cracking, fiber failure, interfacial debonding, and delamination. These can occur separately or interactively, making the study and prediction of composite fatigue behavior difficult. As a result, there is not as adequate a database on composite fatigue properties and performance as there is for metals. This section provides a brief overview of the fatigue process under predominantly tensile fatigue loading, including the damage mechanisms and their effects. For a more in-depth treatment of the topic the reader is directed to References 4-8.

Fatigue damage in composite materials has been defined as the cycle-dependent degradation of internal integrity [4]. This degradation is generally observed as a loss in stiffness and residual strength when the material is cycled at loads lower than the original ultimate strength. The process of damage development is widely dispersed in localized areas. Ultimate failure results when these localized regions have developed an intense enough state of damage to nucleate fracture of the entire specimen. Damage development in composites is dependent upon geometry, mode of loading, material properties and structural arrangement, and environment. Most literature studies have been concerned with fatigue under cyclic tensile loading.

Early work on fatigue of glass reinforced plastics (GRP) has established that matrix cracking is the initial form of damage in multidirectionally reinforced composites [9-11]. The matrix cracks form in resin rich areas between fibers that are aligned perpendicular to, or at large angles to the load direction. As cyclic loading continues, these cracks grow in the matrix and fiber/matrix interface until they reach the fibers of an adjacent layer. If the stress concentrations are great enough, the fibers will break; otherwise, the cracks may propagate along the fiber/matrix interface of the adjacent ply causing delamination. Owen and Dukes, using chopped strand mat, discovered that matrix cracks developed at stress levels as low as 20% of ultimate strength [10]. Chopped mat is

composed of randomly arranged fiber strands rather than plies, and they found that cracks first initiated along fibers, or portions of fibers, lying nearly perpendicular to the load direction.

When Broutman and Sahu [11] studied glass/epoxy prepreg arranged in alternating 0° and 90° layers loaded in the 0° direction, they observed matrix cracks forming at stress levels as low as 10% and 20% of the ultimate strength. At 10% it took several thousand cycles, but at and above 20%, cracks developed on the first cycle in plies oriented at 90°. For plies oriented at 0° (parallel to the load) the stress level had to exceed 75% of the ultimate strength for cracks to initiate on the first cycle. At lower stresses cracks would initiate after a few percent of the specimen life. Furthermore, they observed that the crack density for 90° plies rapidly increased to its maximum value in the first one percent of the lifetime. Crack density in the 0° plies (matrix cracks parallel to the 0° fibers), however, increased rapidly during initial cycling, then leveled off until the late stages of life, whereupon it rapidly increased again prior to complete failure. They also observed that the residual strength of specimens decreased with increasing cycles and that delamination between layers occurred in the later stages of life.

Tanimoto and Amijima [12] examined woven glass cloth and polyester resin in tension fatigue and classified the

progression of damage into three stages. The first stage occupied the first 2% of the lifetime and was characterized by numerous matrix cracks but no decrease in residual strength. The second stage occupied 2% to 50% of the life and was characterized by propagating cracks and a decrease in residual strength as cycles increased. The third and final stage occupied the second half of the life and was characterized by a slowing in the rate of reduction of residual strength until failure occurred. Tanimoto and Amijima observed the same crack density increase behavior as Broutman and Sahu and hypothesized that the large number of cracks in the resin regions acted to relieve high stress concentrations without affecting the residual strength. This hypothesis was later supported by Reifsnider [4].

Dharan [13] also examined the progression of damage using unidirectional glass/epoxy cycled in tension. He classified damage development into three regions based on the slope changes apparent on the S-N (maximum stress versus cycles to failure) curve. In Region I, (<200 reversals) the specimen exhibited an increase in matrix cracks with an increase in applied stress. There were also a large number of fiber failures which coalesced to cause catastrophic failure. The first half-cycle often caused the most damage, with large cracks being produced. In Region II, (200 to 10^6 reversals) matrix cracks developed on the first half cycle and then propagated perpendicular to the applied load. As the cracks

grew they broke fibers, eventually reaching a condition where they moved along the fiber/matrix interface causing interfacial debonding, delamination, and finally catastrophic failure. In Region III, (>10^6 reversals) matrix cracks nucleated after several cycles but no specimens failed. Dharan hypothesized that in this case the applied stress level was below that required to propagate a crack through the glass fibers. The maximum number of cycles in these tests was $2x10^6$.

Recent work by Reifsnider [4] has refined the understanding of damage progression. He, like the other researchers mentioned above, separates fatigue life into three stages for a typical multidirectional laminate: stage I occupies the first 10-15% of life and is characterized by rapid damage development; stage II occupies the next 70-80% of life and is characterized by a decrease in the rate of damage increase; and stage III occupies the final 10-15% of life where the specimen is severely damaged, and continued cycling accelerates damage growth until final failure occurs.

Reifsnider's research has also provided more information on the damage modes present during fatigue. He has found that matrix cracking is present prior to failure in virtually all high-modulus continuous fiber multidirectional composites. These cracks form the basis for other damage which occurs during fatigue. For a given cyclic load level, Reifsnider concurred with Broutman and Sahu that the number of matrix/

cracks reaches a saturation state. Only by increasing the load could more cracks be grown. This saturation state is termed the Characteristic Damage State [4], and is unique to each laminate.

Fiber fractures, the second form of micro damage, occur throughout the fatigue lifetime but can become noticeable within the first third of life. In addition to breaking, these fibers experience local debonding around the newly created tips. As cycling continues these debonded regions can grow along the fiber/matrix interface, leading to interfacial debonding and eventual delamination between plies.

The third form of damage is the development of secondary matrix cracks. These occur in adjacent plies normal to primary matrix cracks and are caused by the stress field around the primary crack tips. Secondary cracks do not develop until later in the fatigue process and are more limited in extent than primary cracks.

The region where primary and secondary cracks cross each other forms the fourth damage mode, local delamination. Delamination is the separating of adjacent plies and is noticeable macroscopically (usually as discoloration in fiberglass reinforced composites) in the latter stages of life. Figure 1 illustrates the fatigue damage process outlined by Reifsnider.

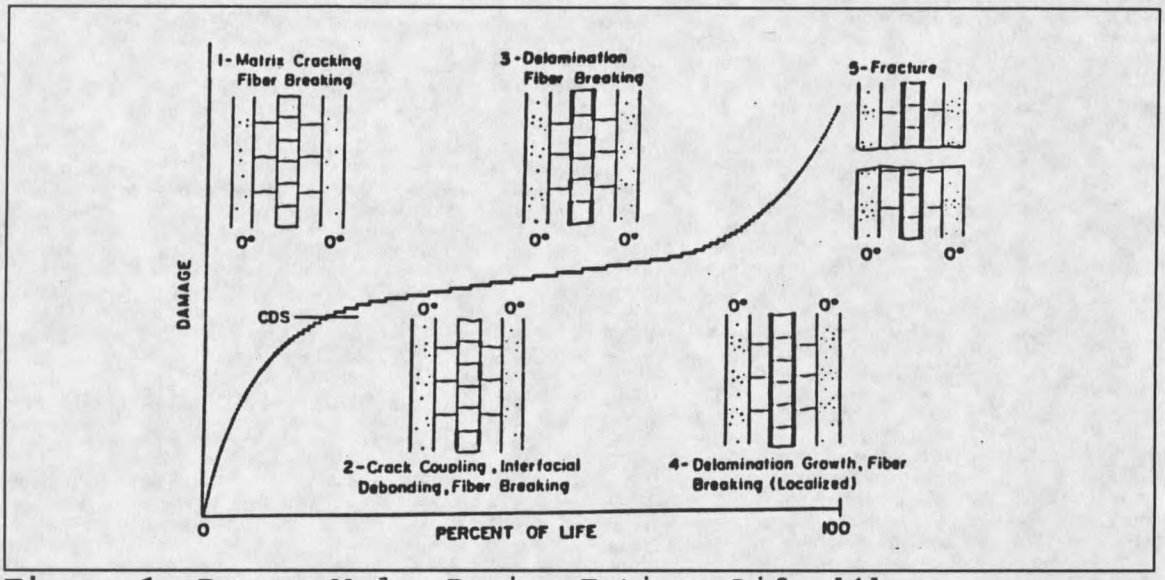


Figure 1. Damage Modes During Fatigue Life [4].

Compression Dominated Fatigue

Compression behavior of composites is not as well understood as tensile behavior. One major reason is sensitivity to test procedures. The method of specimen loading and whether deformation is laterally constrained can produce varying compressive strengths and failure modes. As a result, comparison of data obtained through different testing procedures is difficult. A review of current commonly used compression testing procedures is covered in the following section.

In unidirectional composites, the longitudinal compressive strength is generally lower than the tensile strength. Failure is usually sudden, with very little ply cracking or delamination preceding it. Some factors that influence compressive strength are constituent properties of

the matrix and fibers, fiber diameter and alignment with the applied load, fiber volume fraction, and presence of defects, to name a few [14]. These factors are not much different than those affecting tensile strength; however, compression tests are generally more sensitive to variations in these parameters. Regarding alignment, for example, a five degree fiber misalignment from the load direction was found to cause a 22 percent decrease in compressive strength in graphite/epoxy specimens [14].

Another point of debate with compression is the identification of valid failure modes. In initial work in this area, Rosen [15] modelled a composite as a series of columns (fibers) on an elastic foundation (matrix). As a compressive load was applied to the model, an eventual critical point would be reached when the columns would elastically buckle and the composite fail. This model identified two failure modes, extension and shear (Figure 2). At low fiber volume fractions (below 30%) the extension mode was found to be dominant, while at higher fiber volume fractions (above 30%) shear dominated. However, the drawback with Rosen's model was its consistent over-prediction of

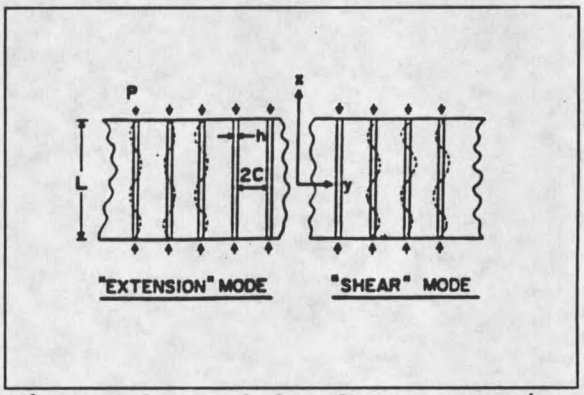


Figure 2. Model of Compressive Failure Modes [15].

compressive strength. Other researchers [14,16] have expanded upon it in an attempt to account for all the factors which effect compressive strength.

Experiments have shown that failure modes are governed primarily by fiber and resin properties [14]. A high fiber modulus coupled with a high matrix shear modulus has been found to produce the best compressive strength [14,16]. Hahn and Williams [16] identified the different failure modes exhibited by fibers, matrix, and the overall composite (Figure

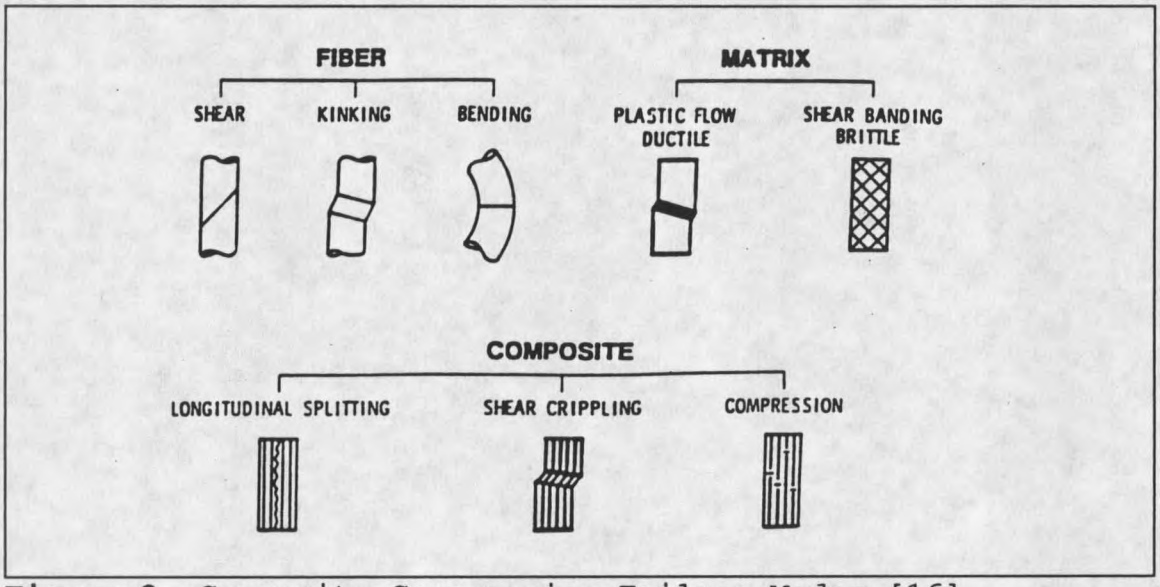


Figure 3. Composite Compression Failure Modes [16].

3). Glass fibers generally fail by bending, and graphite fibers by shear. Greszczuk [14] found that for graphite reinforced composites with low modulus resins, failure was by fiber microbuckling in the shear mode. For intermediate modulus resins, fiber splitting occurred. And for high

modulus resins, fiber compression resulted. Thus, matrix modulus plays a critical role.

Compression fatigue has not been found to be more severe than tension fatigue in glass fiber composites, except that failure occurs at lower cyclic stresses due to the typically lower static compressive strength [7]. If no lateral buckling constraints are used, failure generally results from buckling or microbuckling as described above. If there are constraints, failure can be by compression [4]. The general failure sequence has been observed as local progressive fatigue failure of the matrix near stress concentrations, causing fiber splitting and progressive delamination; this in turn leads to fiber buckling which propagates through the laminate resulting in catastrophic failure [17-19]. Rosenfeld and Huang [17] observed that initial damage was noticeable as delamination between the 0° and off-axis plies, regardless of stacking sequence. However, they noted that delamination occurred sooner when the outer plies were 0°. This finding was supported by Ratwani and Kan [18].

Besides pure tension-tension (T-T) and compression-compression (C-C) fatigue, several studies have also examined the effects of reversed loading, or tension-compression (T-C) fatigue. The general conclusion reached is that T-C fatigue is the most severe [17-19]. Rosenfeld and Huang [17] observed that delamination of the outer plies occurred during both tensile and compressive loading, but that under compressive

loading the delamination progressively became more severe. While technically it is possible for a laminate to fail in either tension or compression, unidirectional specimens under reversed loading have been found to fail predominantly in compression [19]. Furthermore, the slope of the S-N curve in reversed loading is steeper than for T-T cycling with carbon fiber composites, indicating matrix, rather than fiber dominated behavior [19]. For laminates containing unidirectional, angle, and transverse plies, Reifsnider [4] observed both failure modes with carbon/ epoxy. At low stress levels failure was compressive, while at high stress levels it was tensile. This was due to the different ways in which tensile and compressive residual strength change during fatigue.

Compression Test Methods

The list of compression test methods in use today is lengthy. However, the American Society of Testing and Materials (ASTM) specifies only three standardized test methods in the ASTM Test Method for Compressive Properties of Unidirectional or Crossply Fiber-Resin Composites (D3410). These are the Celanese, Illinois Institute of Technology Research Institute (IITRI), and sandwich beam. Many of the other methods in use are modifications of these, or are in-house tests developed for specific applications. This section will provide a brief description of the ASTM D3410 test

methods as well as a few of the modified methods. For a more detailed summary of available compression test options, the reader is directed to Reference 20. All test methods are designed to prevent elastic buckling of the specimen, as distinct from material compressive failure; this is accomplished by using short specimens or lateral constraints which prevent out-of-plane displacements.

The IITRI test is the most versatile of all the ASTM standardized tests. It can accommodate specimens with widths up to 1.5 inches and thicknesses ranging from 0.17 to 0.6 inches. An overall specimen length of 5.5 inches is used, with an unsupported gage section of 0.5 inches. Load is applied through shear by clamping the tabbed specimen ends, as distinct from direct end loading. The test fixture is made of steel and weighs approximately 90 pounds [21]. Specimen alignment is maintained through the use of guide rods between the upper and lower members of the fixture. Linear ball bearings are incorporated to reduce friction. The IITRI test routinely produces the highest compressive strengths with the least amount of scatter [22,23].

The Celanese fixture is more complicated than the IITRI, and has limitations on specimen geometry. Maximum specimen width is 0.25 inches with an unsupported gage length of 0.5 inches. The test fixture is smaller than the IITRI, thus weighing less and being more manageable. The major drawbacks with the Celanese are the high degree of precision required

for coupon geometry , and frictional problems encountered from bearingless alignment rods [20,23]. Some of these problems have been addressed by the Wyoming Modified Celanese fixture. Developed at the University of Wyoming, this fixture allows wider, less precise specimens to be used. Research has shown that the strength values and failure modes produced are very similar to those obtained using the IITRI fixture [21,22].

The sandwich beam is tested in four point bending and is considered by some researchers to be preferable to coupon test methods. This is due to its lack of stress concentrations, uniformity in stress distribution, and demonstrated high, consistent strength and modulus values [22]. The beam is composed of active and passive faces measuring 22 by one inch, separated by a hexagonal aluminum honeycomb core. The active face (test side) is six plies thick, while the passive face consists of 12 plies. The major drawback with this method is the extensive time and cost in fabricating the beam [20].

The other major category of test method involves end-loading, instead of shear loading of the specimen. In these test fixtures, such as the Wyoming end-loaded side-supported, the coupon ends rest on the test fixture, with side grips used only to support the length near the ends which is outside the gage section. There are significant problems with this method because of the failure modes. End crushing and longitudinal splitting occur, causing premature failure and lower ultimate strength [22,23]. Despite these drawbacks, one end-loaded

test is still widely used, ASTM Compressive Properties of Rigid Plastics (D695). Not designed specifically for fiber reinforced composites, the test is used in industry because of its simplicity. Specimen geometry can be a right cylinder, prism, tube, or flat. Flat rectangular specimens are generally used for composites. They measure 3.13 inches long by 1.5 inches wide, and have a 1.5 inch long gage section. Because of this long gage length, lateral buckling constraints are generally employed. However, several modified versions of D695 exist which have reduced gage lengths in order to avoid using lateral constraints.

For fatigue testing none of the methods described above can be used, the primary reason being that they were not designed for repeated cycling. The Celanese fixture has an excessive amount of friction present in the alignment rods. The IITRI fixture, even with its linear bearings, also would develop a significant amount of wear. And the sandwich beam is difficult to run at higher frequencies due to the large displacements. Therefore, compression fatigue testing generally uses coupons similar to those found in tension, with the major difference being a shorter gage length. If a longer gage section is desired, lateral constraints are employed. This is usually the case when reversed loading is studied. However, there is no consensus about the validity or usefulness of data obtained in this manner [7]. Often a circular hole is used to initiate failure in the gage section

for laminates containing angle plies [23,24]. This is impractical with unidirectional layups because longitudinal splitting would result. In instances where torsional stress (induced by piston rotation) is a problem, the actuator head can be rotationally constrained using products designed by equipment manufacturers.

Frequency Effects

When specimens are exposed to cyclic loads, some of the applied strain energy is lost to heat generation. This loss, termed hysteresis, is evident in a stress-strain curve as the area between the loading and unloading curves. In metals, which have excellent thermal conductivity and low hysteresis, this generated heat is small, and is dissipated easily through conduction to ambient air. Polymers, however, are poor thermal conductors, and have relatively high hysteresis. Consequently, the heat generated during cycling is higher, and is not dissipated rapidly. The result is an increase in specimen temperature with increasing stress level and frequency [24-26]. Hysteresis increases rapidly as the stress and stress amplitude increase. This is presently a major limitation in composites testing because at high frequencies the heating can result in thermal, rather than mechanical failure.

Dally and Broutman [24] examined glass/epoxy prepreg arranged in crossply (0°,90°) and quasi-isotropic (-60°,0°,+60°)

laminates to determine the influence of hysteresis heating on fatigue properties. They noticed that hysteresis heating is analogous to heat generation in an electric coil. This led them to the following equation for determining the temperature difference between the surface and the center of a specimen.

$$\theta_{max} = (H/4kE)(a\sigma)^2 f \qquad (1)$$

Here θ_{max} is the difference between the surface temperature and the temperature at the specimen center, H is a material constant, k is the thermal conductivity, E is the elastic modulus, a is the specimen half thickness, σ is the applied stress, and f is the cyclic frequency. This equation shows that for thinner specimens at moderate stress levels the temperature gradient between the surface and the center is less severe. They also concluded that heat was dissipated primarily through convection and only minimally by means of radiation and conduction. This point was later demonstrated by Broutman and Gaggar [25] when they artificially cooled their specimens with air and water. For polyester resin they found that simple forced air cooling could increase specimen fatigue life by a factor of five under some conditions.

Cessna et. al. [26] also used artificial cooling techniques to demonstrate the validity of high frequency testing of glass-reinforced thermoplastics. They ran tests under 'isothermal' conditions at various frequencies (2-37 Hz)

and found that the rate of stiffness decay and the number of cycles to failure were independent of test frequency.

Besides hysteresis heat generation, high frequency testing can affect the mechanical properties of composites. Stinchcomb et. al. [27] studied mechanical properties using boron/aluminum and boron/epoxy specimens tested at frequencies ranging from 0.5 to 45 Hz. They found that for boron/epoxy below 30 Hz there were no major frequency effects on the cyclic stress-strain curve, although there was a slight increase in fracture strain. Above 30 Hz, however, they found significant changes in the cyclic stress-strain curve and a much higher fracture strain. The fracture stress also decreased by a factor of two. Furthermore, the compliance and residual strength of both material combinations increased with the number of cycles, indicating greater amounts of damage. However, there were no consistent trends in frequency effects on compliance and residual strength even though they were different at different frequencies.

Mandell and Meier [28] used E-glass/epoxy prepreg to study the effects of frequency and loading time on fatigue properties. They tested specimens at frequencies of 0.01, 0.1, and 1.0 Hz to avoid hysteresis heating. They found that at higher frequencies specimens had longer fatigue lives. Furthermore, they observed that a specimen run at 0.01 Hz for 100 cycles accumulated more damage than a specimen run at 1.0 Hz for 100 cycles. They concluded that there must be some

effect occurring which is based on time per cycle or total time under load. However, the effects of frequency diminished rapidly at lower stresses and longer lifetimes.

Saff [29] examined the effects of load frequency and lay-up on fatigue life and observed the same increase in life with increasing load frequency that Mandell and Meier did. His experiments showed that laminates with 0° plies were less sensitive to frequency than were laminates with no 0° plies. He also observed that matrix dominated lay-ups were more sensitive to load frequency. Saff felt, however, that fatigue data from tests run at high frequencies were not representative of actual service fatigue where the loading frequency was lower.

The major problem associated with this argument is the extensive amount of time needed to run fatigue tests at low frequencies (as discussed in Reference 30 which shows relatively small frequency effects when hysteresis is not an issue, especially at long lifetimes). For a project such as this one where data out to 10^8 cycles are desired, it could take years to obtain a single S-N (stress versus number of cycles to failure) curve, and this is assuming no mechanical problems with the testing equipment. Therefore, testing at high frequencies is desirable. Research by Creed [3,31] demonstrated that high frequency (100 Hz) tensile testing can be accomplished, and that the resulting data correlates with previous work done at lower frequencies. Creed was able to

achieve success by testing smaller volumes of material instead of standard sized coupons. These smaller specimens had the advantage of much better heat transfer characteristics because of their extreme thinness, and they still retained the overall material properties observed in standard size coupons. Surface temperature measurements and finite element analysis verified the improved heat transfer characteristics and the validity of the specimen geometry.

CHAPTER THREE

EXPERIMENTAL METHODS

Mechanical Testing Equipment

A high response, low force Instron Model 8511 servohydraulic test machine, capable of generating 2000 pounds

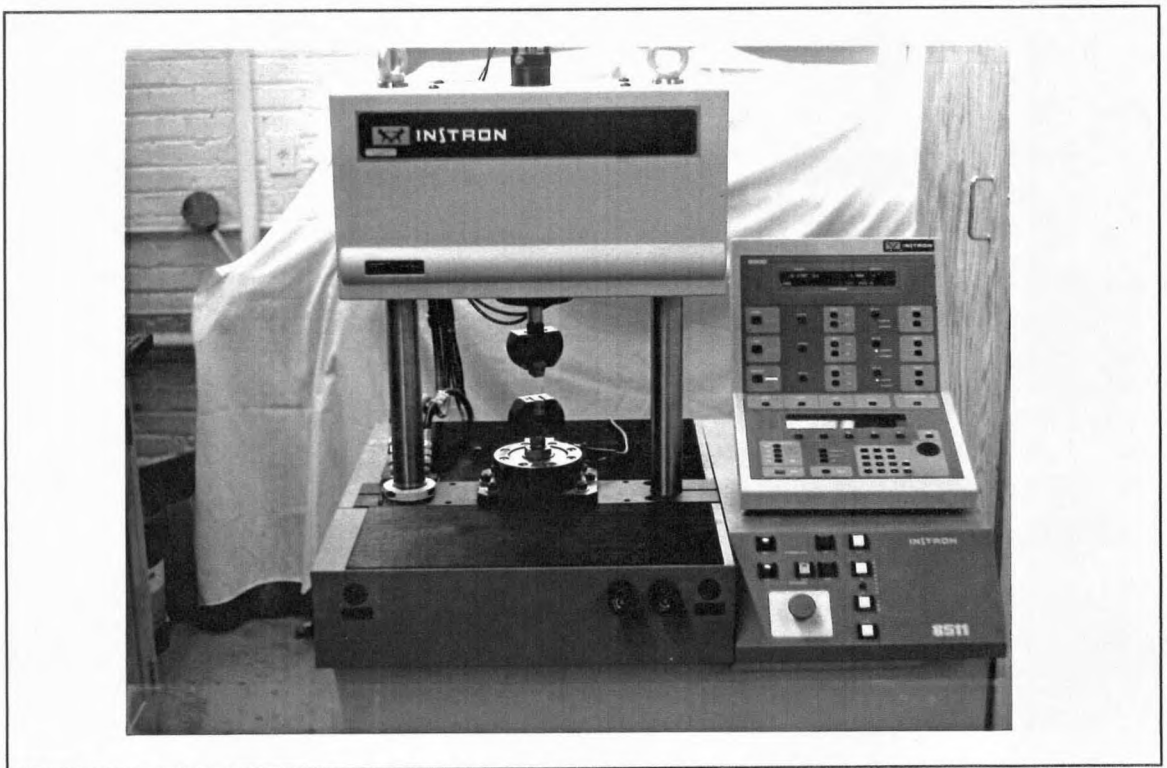


Figure 4. Instron 8511 Servohydraulic Test Machine.

of force, was used for static and fatigue testing (Figure 4). A 5000 pound range load cell was employed. Piston displacement was measured with a linear variable differential

transducer (LVDT). The 8511 was selected because it is capable of accurately applying low loads (less than 10 pounds) and running at very high frequencies (in excess of 100 Hz) at adequate displacements. It has a 10 gallon per minute (GPM) servo valve and operates at 3000 psi hydraulic pressure supplied by a 20 GPM pump.

All tests were conducted under load control. Static tests were controlled from a personal computer using Instron Series IX software. Static loading rates were consistent with a fatigue test frequency of 20 Hz. Specimen series run at different R values (minimum stress/ maximum stress) were tested at the same loading rate, allowing valid data comparison between data sets. The loading rates ranged from 28,000 to 30,000 pounds per second. Strain was measured using Micro-Measurements EA-06-062AP 350 ohm strain gages and an Instron ±0.1 inch displacement extensometer Model Number 2620-826.

Fatigue tests were controlled through the 8500 digital control panel. All tests were run with constant force amplitude sine waves. The amplitude and average load were determined from the R value and minimum (most compressive) stress level of each test. Test frequencies were varied with stress level in order to maintain a constant average loading rate. Furthermore, at the beginning of a test the amplitude was increased gradually to avoid damaging the specimen with a possible overload on the first cycle. This was very important

at higher frequencies where the initial load application could have caused excessive damage. Waveform quality was monitored with an analog oscilloscope. Specimen surface temperatures were measured with Omega Tempilaq liquid crystal paints which melt at specific temperatures.

Specimens were loaded by clamping in grips developed in this research. The Appendix contains a description of the grips used. No anti-buckling constraints were employed. Instead, specimen gage length was sufficiently short to avoid elastic buckling.

Experiments were conducted in ambient air with temperatures ranging from 65 to 80 degrees Fahrenheit and generally low humidity.

Specimen Fabrication

Specimens were fabricated from Hexcel 0155-50 unidirectional E-glass cloth (Figure 5) and Corezyn 63-AX-051 orthopthalic polyester resin. Densities of the materials were 2.54 g/cc for E-glass and 1.2 g/cc for polyester (information provided by manufacturers). The catalyst for the resin was 2% methyl ethyl ketone peroxide (MEKP) by volume.

Fabrication was carried out through resin transfer molding (RTM). The procedure described here was developed in accompanying research by Hedley [32]. In RTM, catalyzed resin is injected into a mold containing dry fiber reinforcement arranged in desired orientations. The mold used in this

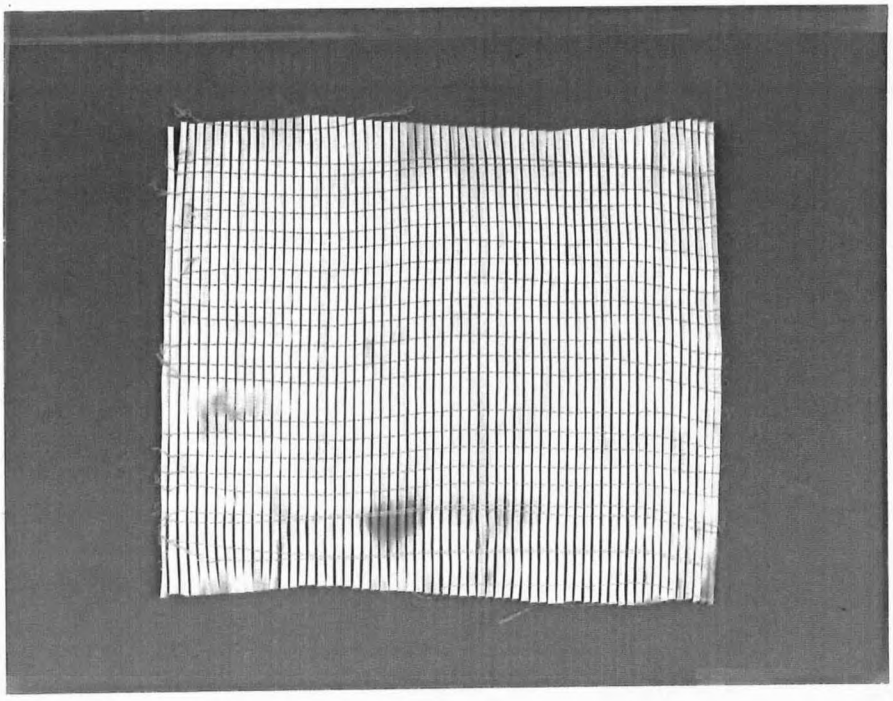


Figure 5. Hexcel Unidirectional E-glass Cloth No. 0155-50.

research was flat, measuring 18 inches long by seven inches wide. It consisted of a 0.25 inch thick aluminum bottom plate with one injection port and two exit vents. The surface was polished smooth with 2400 grit sandpaper to reduce adhesion of cured material. The other side of the mold was 0.25 inch thick tempered glass. This was used to allow monitoring of the injection process. Tempered glass was chosen because normal glass could not handle the high stresses which resulted from a combination of clamping pressure and internal injection pressure. Around the edges was a rubber gasket seal measuring approximately 0.035 inches thick and 0.5 inches wide. Varying the gasket thickness produced different specimen thicknesses and fiber contents. Fiber Resin Corporation FR-1000 silicone

mold release was applied to both sides of the mold prior to loading the reinforcement.

For unidirectional fiberglass cloth it was necessary to leave a 0.5 inch wide empty section across the front of the mold over the injection port. This allowed the resin to cover the entire width of the mold before moving into the reinforcement. It was observed that if no fiber-free band was left over the injection port, resin would flow down to the exit vents only in the center of the mold; the resin had a very difficult time crossing the fibers to reach the sides. Three one inch angle irons were clamped across the tempered glass to ensure uniform composite plate thickness by preventing glass bulging. The whole apparatus was clamped together with 12 C-clamps torqued to 30 inch-pounds. A Cole Parmer Masterflex peristaltic pump capable of generating 25 psi of injection pressure was connected to the mold by silicone rubber tubing. Injection was done slowly to avoid fiber movement and gasket failure, taking approximately 15 to 20 minutes. Once resin reached the exit vents the pump was turned off. Before clamping the injection and vent tubes, the pressure in the mold was allowed to equalize in order to reduce any mold deformation which would result in a non-uniform thickness plate [32]. Figure 6 illustrates the RTM setup.

The curing composite plate was kept in the clamped mold for approximately one hour (longer if the ambient air

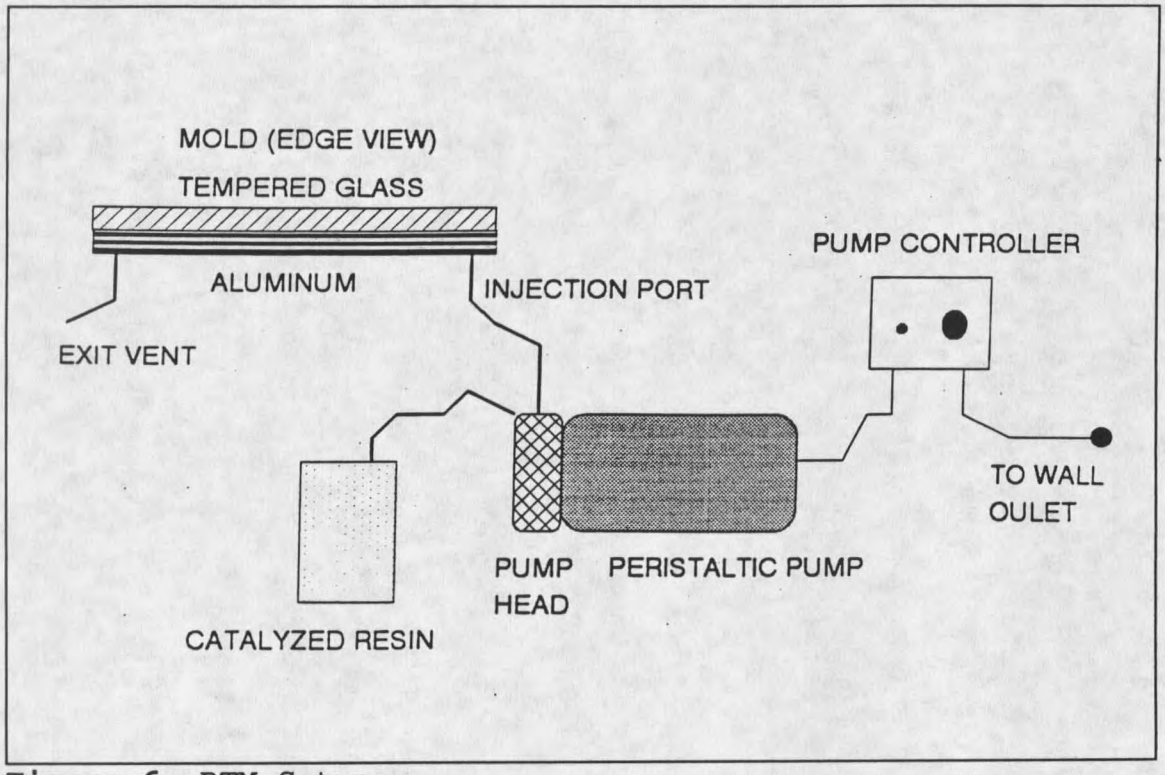


Figure 6. RTM Setup.

temperature was below 70°F). This time was chosen because it was found that the composite was not completely cured and therefore not very brittle. This made removal from the mold easier and preserved the composite quality by reducing the possibility of cracking. The composite was then placed in an oven at 140°F to postcure for approximately two hours. While in the oven the plate was kept in the unclamped mold to prevent warping.

Quarter inch wide specimens were cut from the cured plate using a diamond tipped, water cooled table saw blade. This is the same specimen width used by Creed [3] in previous work. An attempt was made to ensure that three complete fiber bundles (Figure 5) in each layer were included across the

width of each specimen, but differences in fiber packing made this goal difficult to achieve on a consistent basis. As a result, fiber distribution and fiber volume fraction were found to vary between specimens. An explanation of how these differences were measured is contained in a following section. Tabs were cut from sheets of Plastifab (0°/90°) fiberglass/ epoxy mat and were bonded onto the specimens using Hysol EA 9309.2NA epoxy. All bonded surfaces were sanded with 320 grit sandpaper, washed with water, then rinsed with acetone. The sanding roughed up the smooth surfaces and eliminated the layer of silicone mold release on the composite, allowing the epoxy to adhere more reliably. Tabbed specimens were placed in an oven at 140°F for 12 to 24 hours to ensure complete adhesive curing. Prior to being placed in the grips, the tabs were sanded flat and parallel using a granite stone covered with 320 grit sandpaper. This ensured that the tabs were gripped evenly.

Chapter 4 also describes modifications to Creed's [3] tensile test specimens. These Specimens were then used to generate tensile fatigue data for the materials used in this study.

Porosity Measurement

Specimen porosity content was measured using a Leitz Wetzlar light microscope connected to a Sony 13 inch monitor by a Panasonic CL110 color video camera. Cross sections of

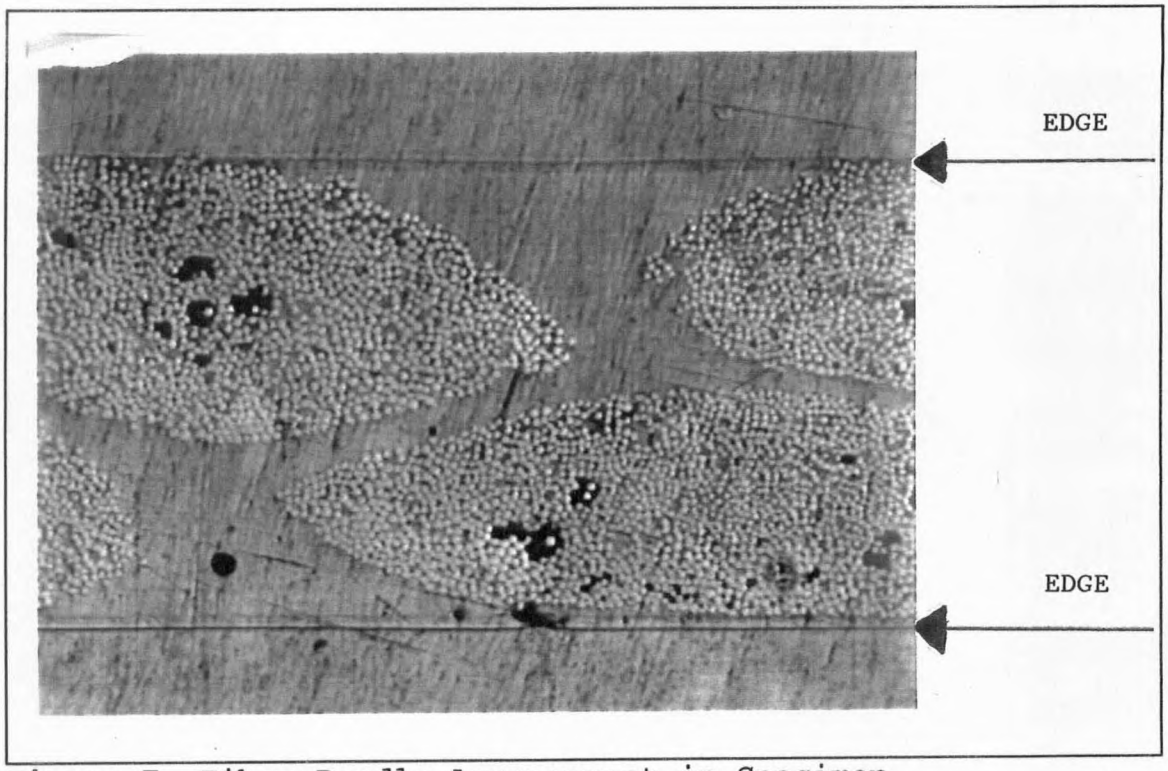


Figure 7. Fiber Bundle Arrangement in Specimen.

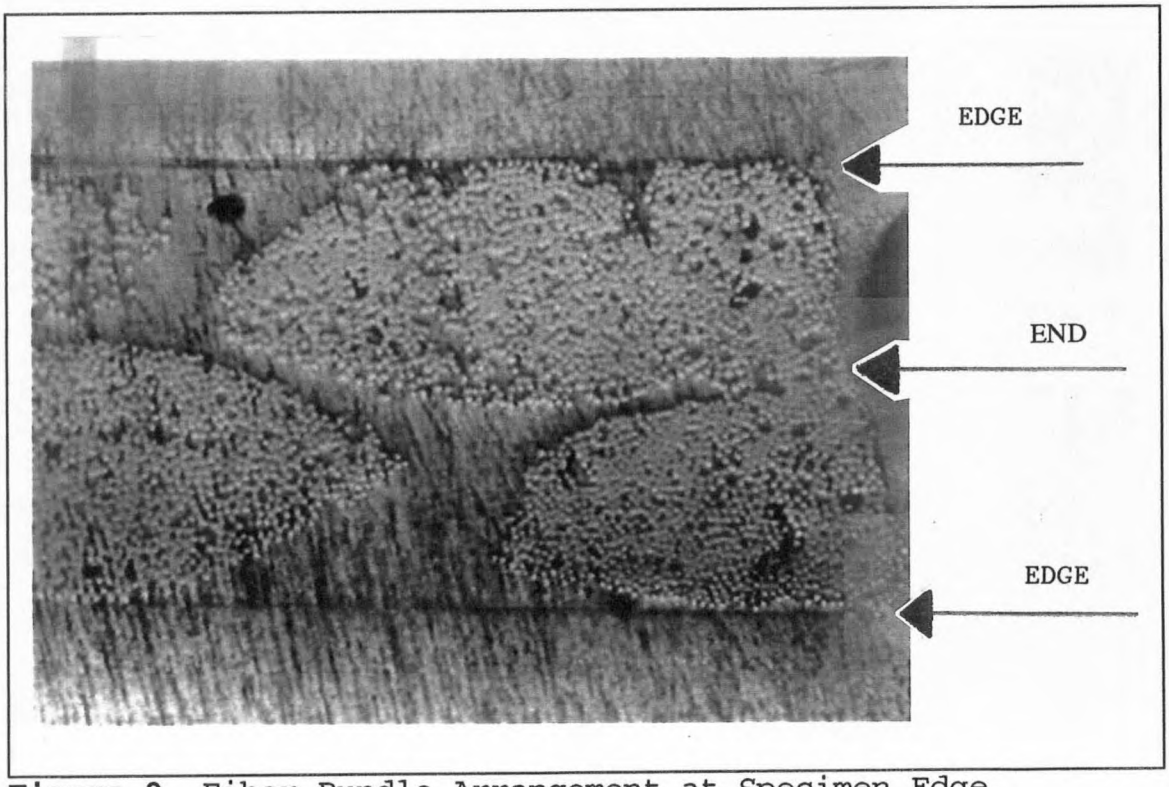


Figure 8. Fiber Bundle Arrangement at Specimen Edge.

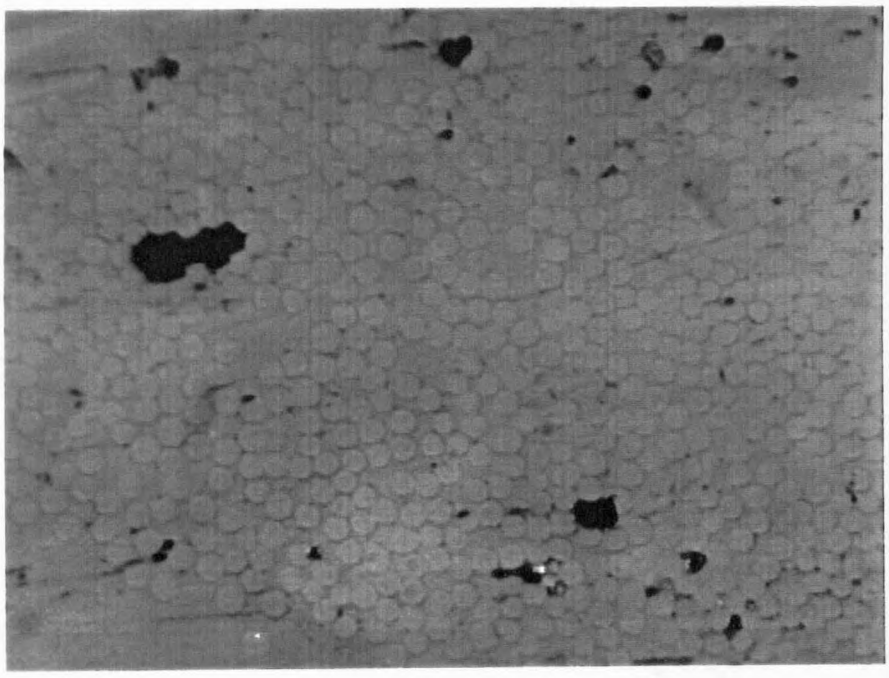


Figure 9. Fiber and Pore Arrangement in Fiber Bundle.

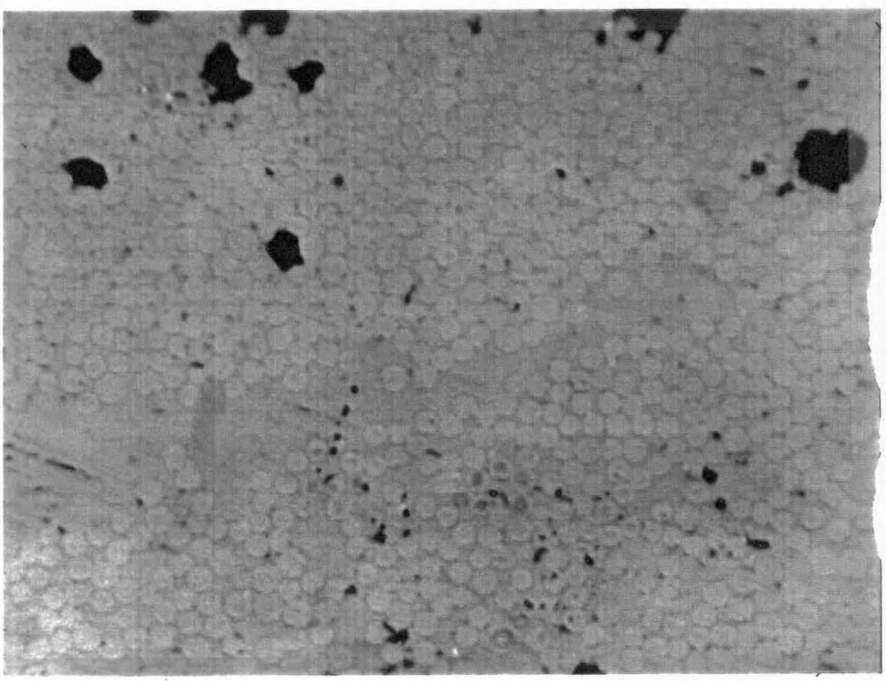


Figure 10. Fiber and Pore Arrangement in Fiber Bundle.

specimens were potted in 1.5 by 0.75 inch Buehler epoxy resin disks. These were polished using 240, 800, 1200, 2400, and 4000 grit sandpaper until fiber ends could be clearly distinguished. Porosity was determined by counting the fraction of grid intersections in a 79 by 57 line grid (81 intersections per inch) that landed on voids, following Reference 33. The grid was placed over the video screen. A magnification of 193X was used to measure porosity for all cross sections. This procedure was repeated for several different regions in a cross section and in a composite plate. Porosity values ranged from 2.14% to 4.0% for the specimens used in this research. Figures 7-10 are light microscope photographs of the internal arrangement of fiber bundles and locations of pores in cross-sections. It can be observed in Figure 8 that at the edge of a specimen, a fiber bundle has been partially cut. This illustrates the problem described earlier with attempting to ensure that three fiber bundles in each layer were included in the width of each specimen.

Fiber Content Measurement

Fiber volume fraction was measured by burning off resin from a representative section of composite plate, consistent with ASTM Standard D3171. The piece was dried and weighed and then placed in a Hevi Duty 051-PT oven heated to approximately 1100°F. Following total oxidation of the resin, the remaining glass fibers were weighed. Volumes were determined using the

densities provided by the manufacturers. The fiber volume fraction of the composite plate used was 48%. However, the fiber volume fractions of each specimen cut from this plate were found to vary because of the fiber bundle packing differences described earlier. Measurement of these variances was made in two ways. One was by the grid method described above to measure porosity content. The other involved polishing the ends of each specimen and counting the number of fiber bundles present (fractional bundles were taken into account). By knowing the weight of a fiber bundle per unit length and the volume of a specimen gage section, the fiber volume fraction was obtained. It was determined that the fiber volume fraction did not change significantly (approximately one percent) between the end of a specimen and the gage section. Therefore, fiber contents for individual specimens were determined by polishing the fiber end. The effects of these varying fiber contents are discussed in Chapter 4.

Fracture Surface Examination

Fracture surfaces of static and fatigue specimens were examined using a JEOL 6100 scanning electron microscope with a LaB_6 filament. An electron beam intensity of 8 KeV was found to provide the best resolution. The fracture surfaces were coated with a 25 nm layer of gold/palladium due to the low electrical conductivity of the specimens.

CHAPTER FOUR

RESULTS AND DISCUSSION

Test Development

Compression

In the course of developing a test method for high frequency compression fatigue testing it was necessary to replace the grips on the Instron 8511. The ones used in previous work by Creed [3] did not perform well in compression; specimens slipped and were aligned slightly off-center relative to the applied load. This induced a bending moment which caused buckling and affected specimen performance. The Appendix contains information pertaining to the grips used in this research.

The compression specimen geometry used in this research was selected after experiments with several other geometries. It was necessary to make the specimen as thin as possible in order to preserve good heat transfer so high frequency tests could be run. Also, it was observed that the higher loads required for thicker specimens caused tabs to debond.

Several iterations of the development process were conducted before a suitable specimen geometry was determined. The main problem encountered was that early designs worked

well in single cycle static tests but performed poorly in fatigue.

The first specimen design used four plies of the roving used by Creed [3], and was manufactured by compressing the fibers and resin together in an aluminum mold cut to the width of the fiber roving (0.25 inches). These specimens had a high degree of fiber misalignment due to the inherent waviness present in the roving. It is believed that the waviness resulted from the winding method used to store the material on spools. The specimens were tabbed with a 0.125 inch wide piece of teflon between the tab and the composite next to the gage section as in [3]. The teflon was used to provide a load transition zone between the glued tab and the gage section. In fatigue testing, however, the specimens failed behind the teflon at the glue/ composite boundary. Figure 11 illustrates the failure mode observed.

In an attempt to produce valid compressive failure modes in the gage section, the roving was replaced with three plies of unidirectional cloth. This was done to remove any possible effects of misaligned fibers. It was felt that these potential non-uniform regions could act as initiation sites for specimen failure. The unidirectional cloth specimens with a decreased thickness reduced the amount of force that had to be transferred to the composite through the tabs, thereby reducing the possibility of tab debonding. Teflon was still used at the edge of the gage section to provide a load

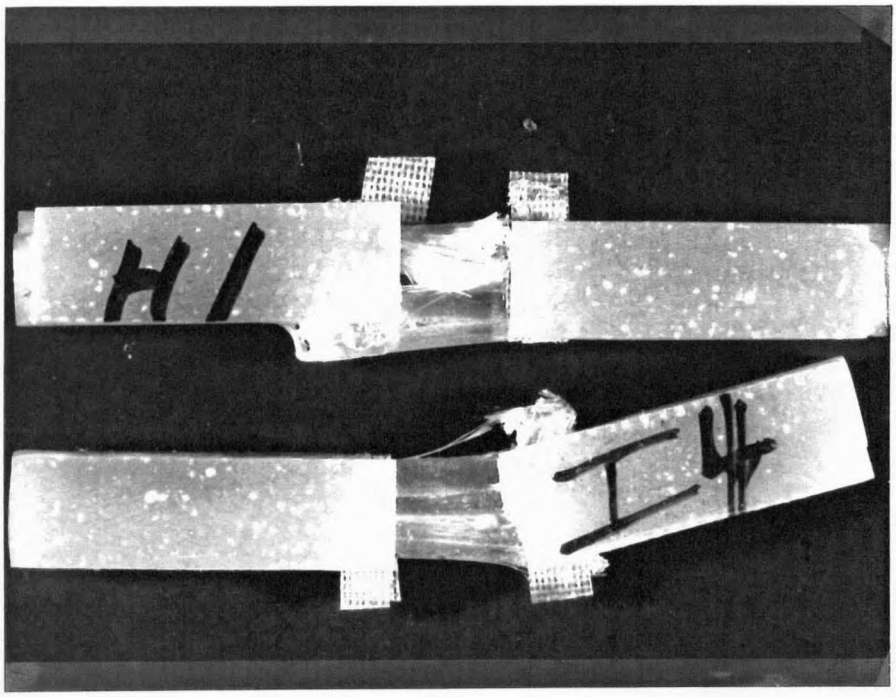


Figure 11. Failure Mode for Early Specimens with Four Plies of Roving.

transition zone. Failure, however, still occurred behind the teflon at the glue/ composite boundary. Figure 12 illustrates the failure mode observed.

The next major alteration to specimen geometry was to reduce the number of plies to two. This was done to further reduce the force that had to be transferred through the tabs. Teflon was still used to act as a load transition zone. Failure, however, still occurred behind the teflon.

At this point several different tabbing methods were examined. One involved replacing the teflon with silicone in order to produce a load transition zone that was stiffer than the teflon but not as rigid as the epoxy glue. This method

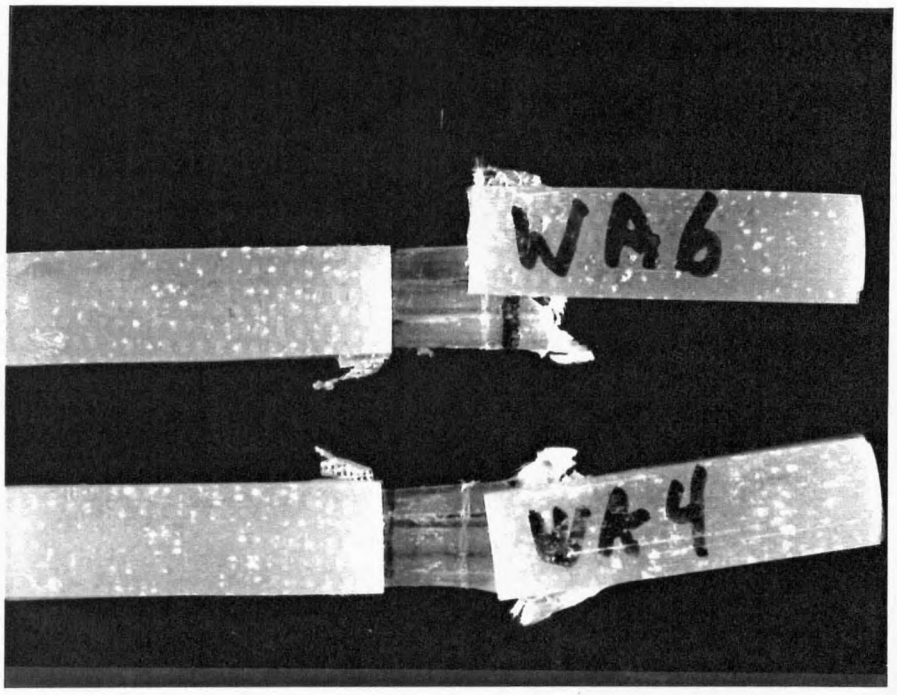


Figure 12. Failure Mode for Three Plies of Unidirectional Cloth.

was not successful and failure still occurred at the epoxy/ composite boundary. Another method involved tapering the tabs and bonding them onto the composite without using a second material to act as a load transition zone. This method failed because the specimen could not be gripped to the edge of the gage section. The result was an unsupported area that was twice as long as the gage section causing buckling to occur. Finally, square tabs with no teflon were employed, and as discussed later, specimens usually failed in the gage section, supporting the use of this design. The use of square tabs is questionable in terms of stress concentrations. However, finite element analysis by Creed [3] showed that the stress

concentration which exists around a square ended tab in a geometry and thickness similar to the one used here extends only several fiber diameters into the composite. Therefore, the effect on overall specimen behavior was not expected to be great.

Specimen geometry was 0.25 inches wide by 2.2 inches long by approximately 0.035 inches thick (see Figure 13). The thin specimens required a short gage length of 0.2 inches (roughly five times the specimen thickness of 0.035 inches) to avoid elastic buckling. Tabs measured 0.25 inches wide by one inch long by 0.06 inches thick. The tab length of one inch was

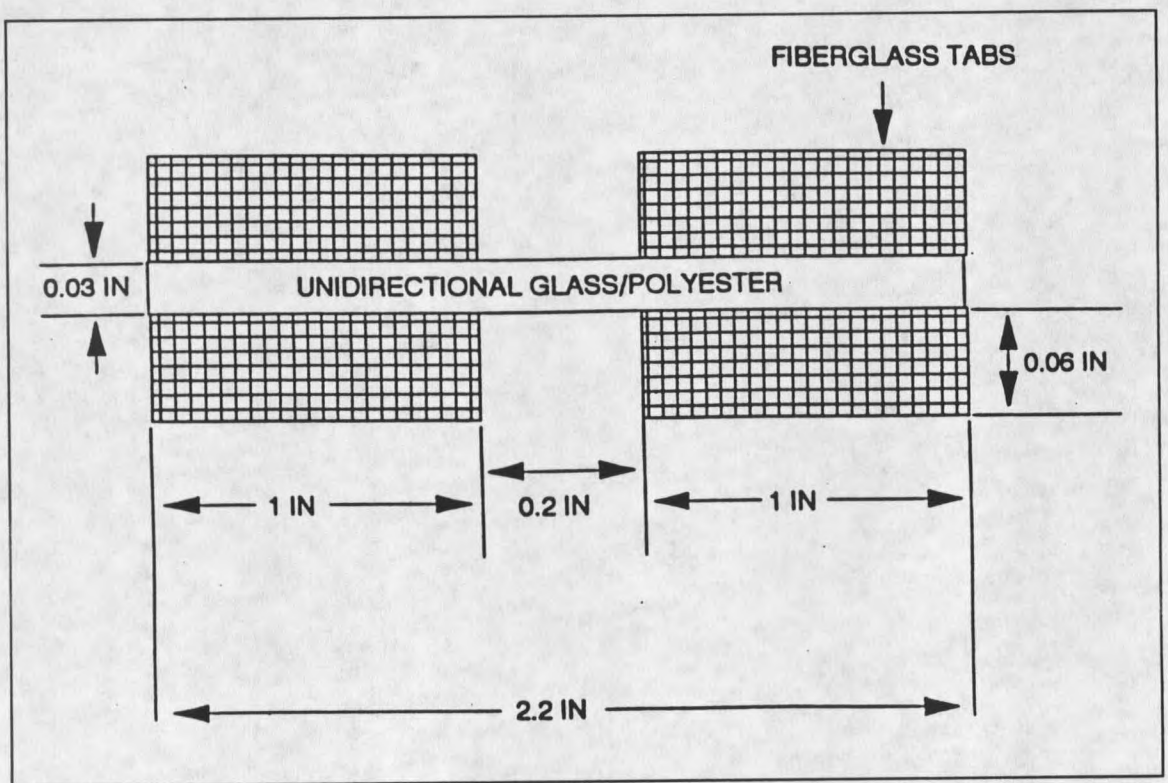


Figure 13. Compression Specimen Geometry.

used to provide adequate surface area for load application, as well as to enable specimen alignment.

It was observed (as was discussed earlier in the background section) that specimen alignment is critical to valid compression testing both statically and in fatigue. Figure 14 illustrates the difference in specimen behavior between misaligned and aligned specimens at R=10, observed in this research. The misaligned specimens were either not centered under the applied load correctly, or the fibers were not completely parallel to the applied load direction. The result of this improper alignment was increased scatter and premature fatigue failures. To ensure proper alignment during testing, lines were etched in the grips directly under the center of the applied load. These marks were then lined up with the center of the specimen. Care was also taken to ensure that the bottoms of both jaws on a gripface were even (see Appendix). If they were not, the specimen ends would not be aligned vertically, and a bending moment would be introduced.

The two-ply glass/ polyester material was characterized using a compressive stress-strain test performed at a lower loading rate of 25 pounds per second. The modulus from this curve (Figure 15) was 5.14 msi, and this value was used to calculate the initial peak strains experienced by specimens during fatigue testing. The ultimate compressive strength was 95,526 psi, and the strain to failure was 1.67%. The fiber

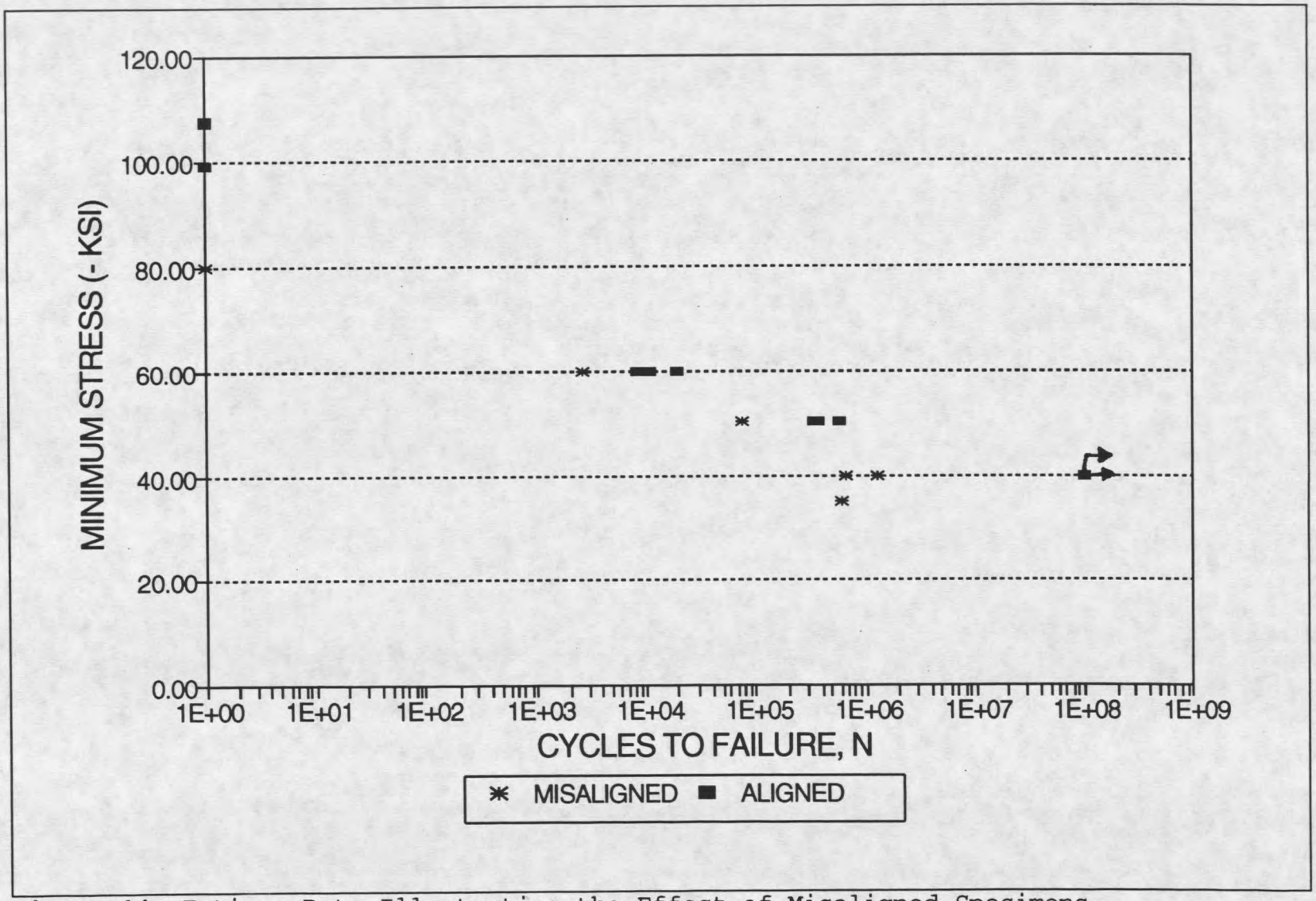


Figure 14. Fatigue Data Illustrating the Effect of Misaligned Specimens.

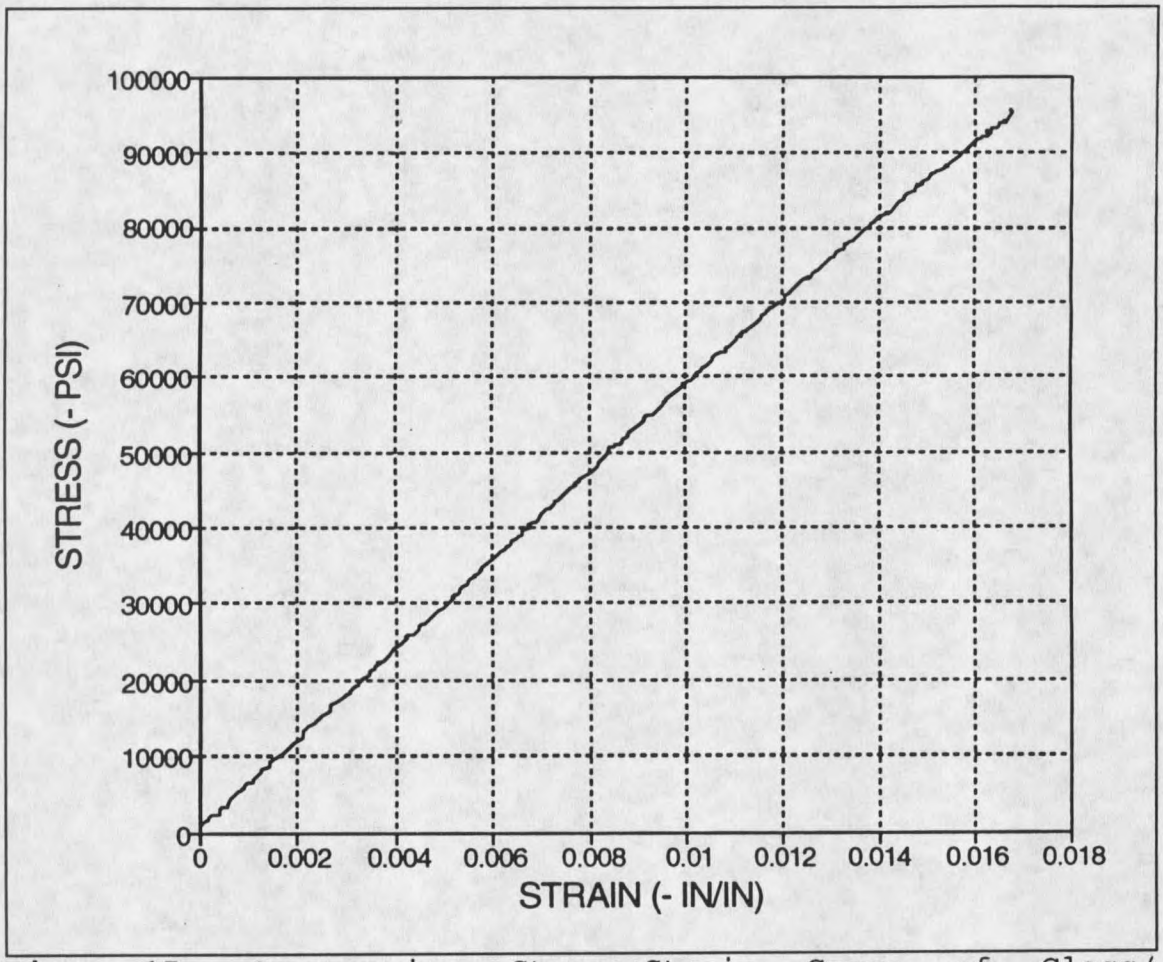


Figure 15. Compressive Stress-Strain Curve of Glass/ Polyester.

volume fraction of this specimen was 52%.

Tensile Fatigue

The earlier work in high frequency tensile fatigue by Creed [3] used relatively low strength (95 ksi) material with a wavy geometry in the strands. Creed's work was extended in the present study to include tensile fatigue testing of stronger, well aligned material. Specimen development in this phase of research focused primarily on designing a specimen geometry that prevented tab debonding (there were no problems

with failure location). The same two-ply well-aligned glass/ polyester material was used for the tensile specimens as was used for the compression specimens. Initially the same specimen geometry was used in tension as was used in compression. However, it was observed that when tabs were bonded directly to the composite, debonding occurred after the first few fatigue cycles. This was due to the higher ultimate strength of the well-aligned material compared to the roving used by Creed. To deal with this difference, two alterations were made to the tensile specimens. First, one ply of cured 3M SP-250E unidirectional E-glass/ epoxy prepreg (0.005 inches thick) was bonded to the composite in the tab regions. The gage section (0.2 inches in length) was not covered. Then the tabs (same dimensions as in compression) were bonded onto the prepreg. The prepreg extended beyond the tabs 0.1 inches and was tapered to zero thickness at the edge of the gage section. The distance between tabs was 0.4 inches. Second, the gage section thickness was tapered down from 0.035 to 0.015 inches (approximately one ply thickness) in the center. Tapering was accomplished using a Dremel Moto-Tool Model number 395 with a 0.7 inch diameter grinding bit, yielding a radius of curvature of the tapered region of 0.35 inches, and a uniform thickness across the width of the gage section. The tab stepping arrangement introduced load gradually into the gage section and reduced the stress concentrations which caused tab debonding in the earlier test geometry. Figure 16 illustrates

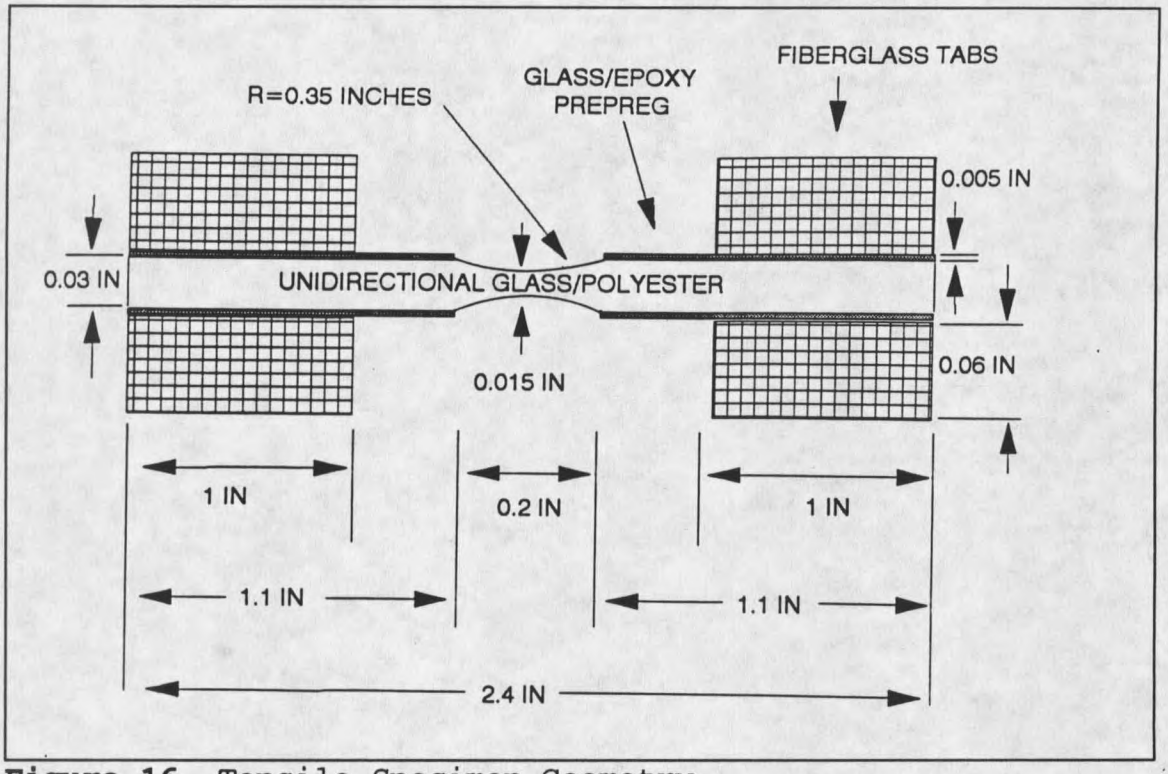


Figure 16. Tensile Specimen Geometry.

the tensile specimen geometry used. The material was characterized using a tensile stress-strain test performed at a loading rate of 25 pounds per second (see Figure 17). An untapered specimen was used because it was impossible to strain gage the small, non-flat tapered section of the tensile fatigue specimens. The modulus of the material was 6.7 msi and this value was used to calculate the initial peak strain levels for the tensile fatigue tests. This modulus is most likely low because the tapered specimens are believed to have a higher fiber content due to the tapering process. The ultimate tensile strength was 153,017 psi and the strain to failure was 2.3%. The fiber volume fraction of the untapered stress-strain specimen was 67%.

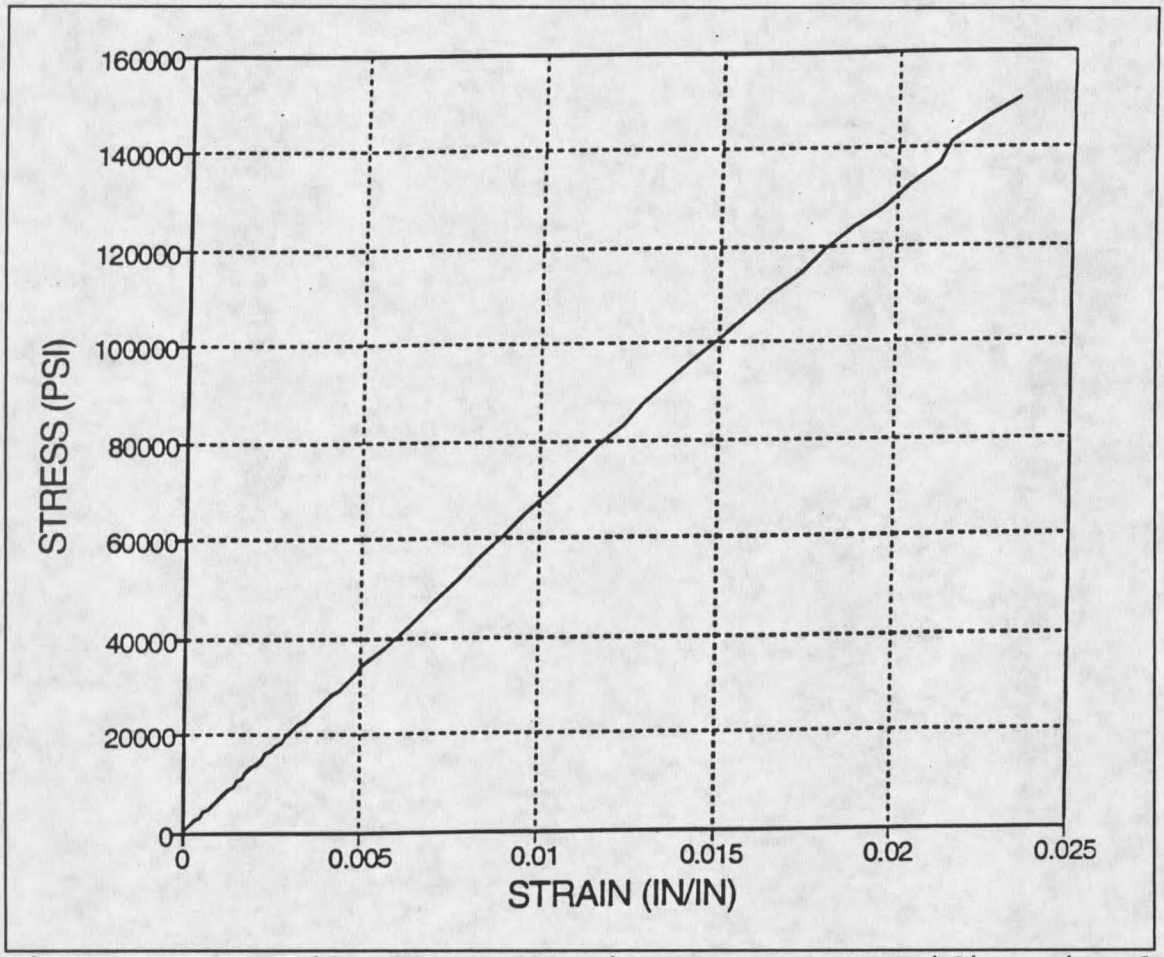


Figure 17. Tensile Stress-Strain Curve for Unidirectional Glass/ Polyester.

Fatigue Results

Three different R values (minimum testing stress/ maximum testing stress) were tested in this research, R=10, R=2, and R=0.1. Figure 18 illustrates the relationships of the testing sine waves for the three R values on a plot of stress versus time. (Note that the minimum stress is taken as the greatest compressive stress in compression fatigue, since compression is taken as a negative stress.)

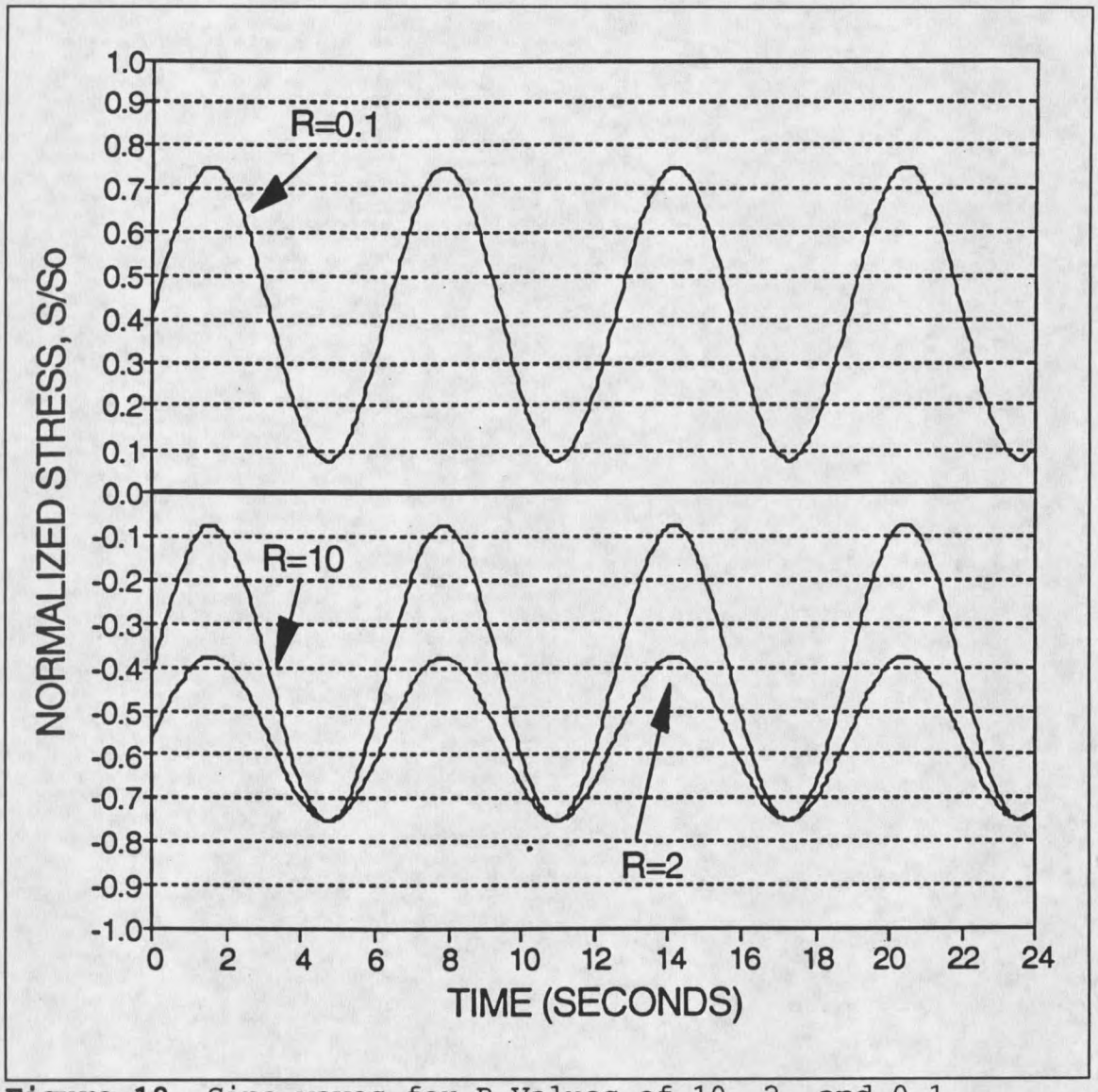


Figure 18. Sine waves for R Values of 10, 2, and 0.1.

Compression

Figure 19 shows normalized S/N (stress versus number of cycles to failure) data obtained at an R value of ten. The data show relatively little scatter, and the runouts at 10^8 cycles were tested at an initial minimum strain of about 0.8%.

The S/N data are in approximate agreement with an 8% decrease in stress level to obtain a decade of increased lifetime which is typical for compression fatigue of continuous fiber composites [34]. Compression failures are usually matrix dominated, and both neat resins [30] and composites with various layups [35,36] have been found to approximately follow the 8% per decade line. Furthermore, both glass and carbon composites show similar compressive fatigue behavior [37,38]. However, data for unidirectional composites tested in compressive fatigue (in both glass and carbon composites) are scarce. Table 1 contains raw data for the R=10 curve. The points out to 10^8 cycles represent the first known published data obtained in this cycle range. Testing time for these specimens was on the order of 11 days.

The validity of the high frequency test results is also supported by a comparison with data from large coupons fabricated from the same material as the high frequency specimens, but run at lower frequencies (10-20 Hz). Figure 20 compares normalized R=10 data obtained in this research with normalized R=10 data obtained in accompanying work by Combs [39]. The standard sized coupons used by Combs were 48% fiber volume fraction, and composed of 67% unidirectional fibers and 33% ±45° fibers. It was necessary to use some off axis plies because of the difficulty in testing standard coupons of unidirectional fiberglass composites in compression due to tab related failures. The larger coupons tend to follow the 8%

Table 1. Data for R=10 S/N Curve.

Minimum Stress (ksi)	Test Frequency (Hz)	Initial Peak Strain (%)	Cycles to Failure
-107.6	30,487 lbs/sec	-2.09	1
-107.5	30,457 lbs/sec	-2.09	1
-99.1	28,083 lbs/sec	-1.93	1
-60	40	-1.17	8226
-60	40	-1.17	10,886
-60	40	-1.17	19,210
-50	60	-0.97	337,992
-50	60	-0.97	375,478
-50	60	-0.97	587,407
-40	100	-0.78	1.03E+08 *
-40	100	-0.78	1.04E+08 *

* signifies a run-out (no failure)

per decade line more closely than do the high frequency specimens (especially in the 10^4 to 10^5 cycle range), but overall the data are in good agreement. Thus, the high frequency data using small unidirectional specimens yield S/N data which predict the normal laminate coupon data when the stresses are normalized by the initial compressive strength. This is despite a significant difference in static strength (-61 ksi versus -105 ksi).

A least squares power law fit (including runout points) was found to provide the best fit to the data in Figure 19 (R^2=0.9938). The reasons for the differences in trend lines between the small high frequency specimens and the standard

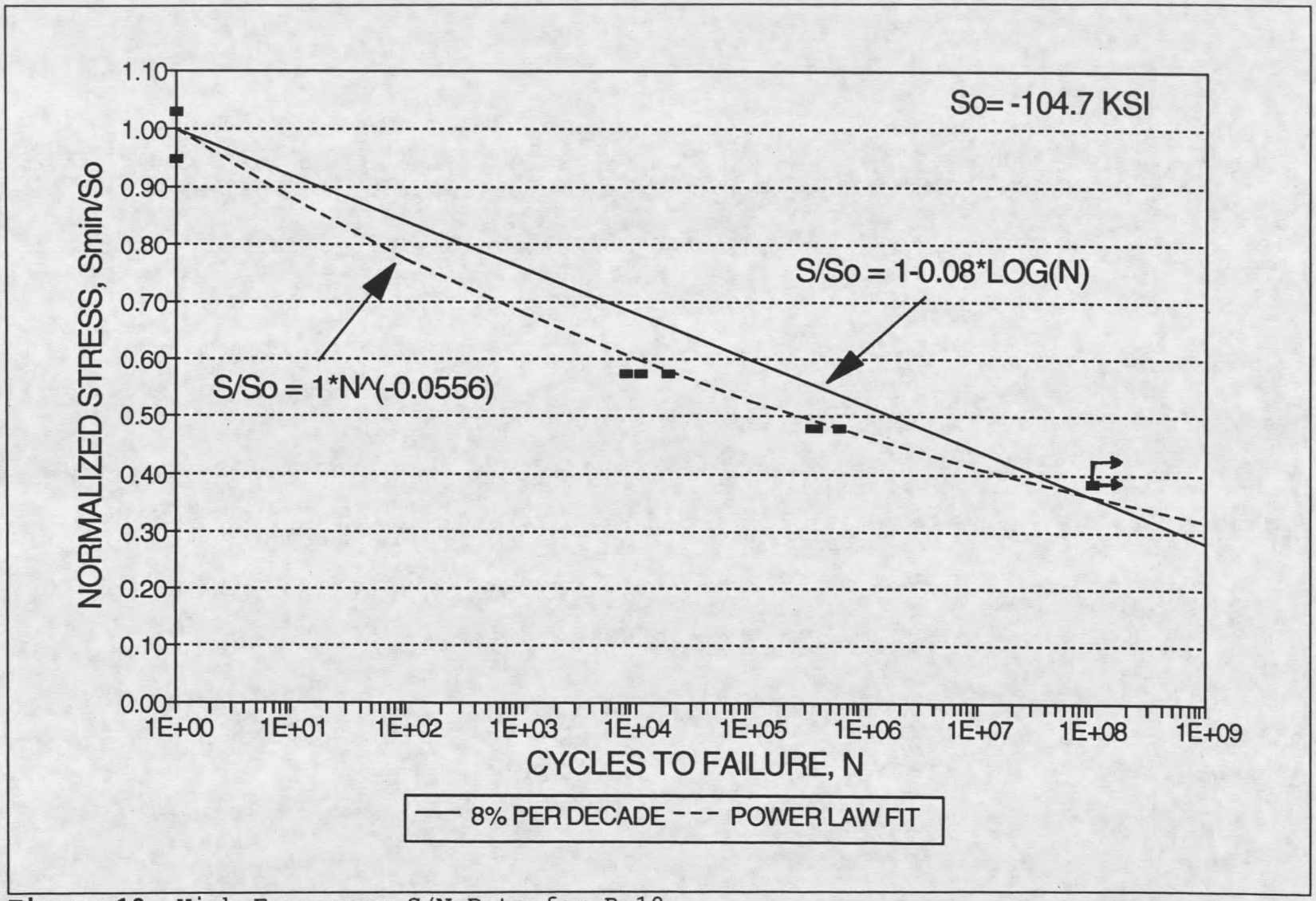


Figure 19. High Frequency S/N Data for R=10.

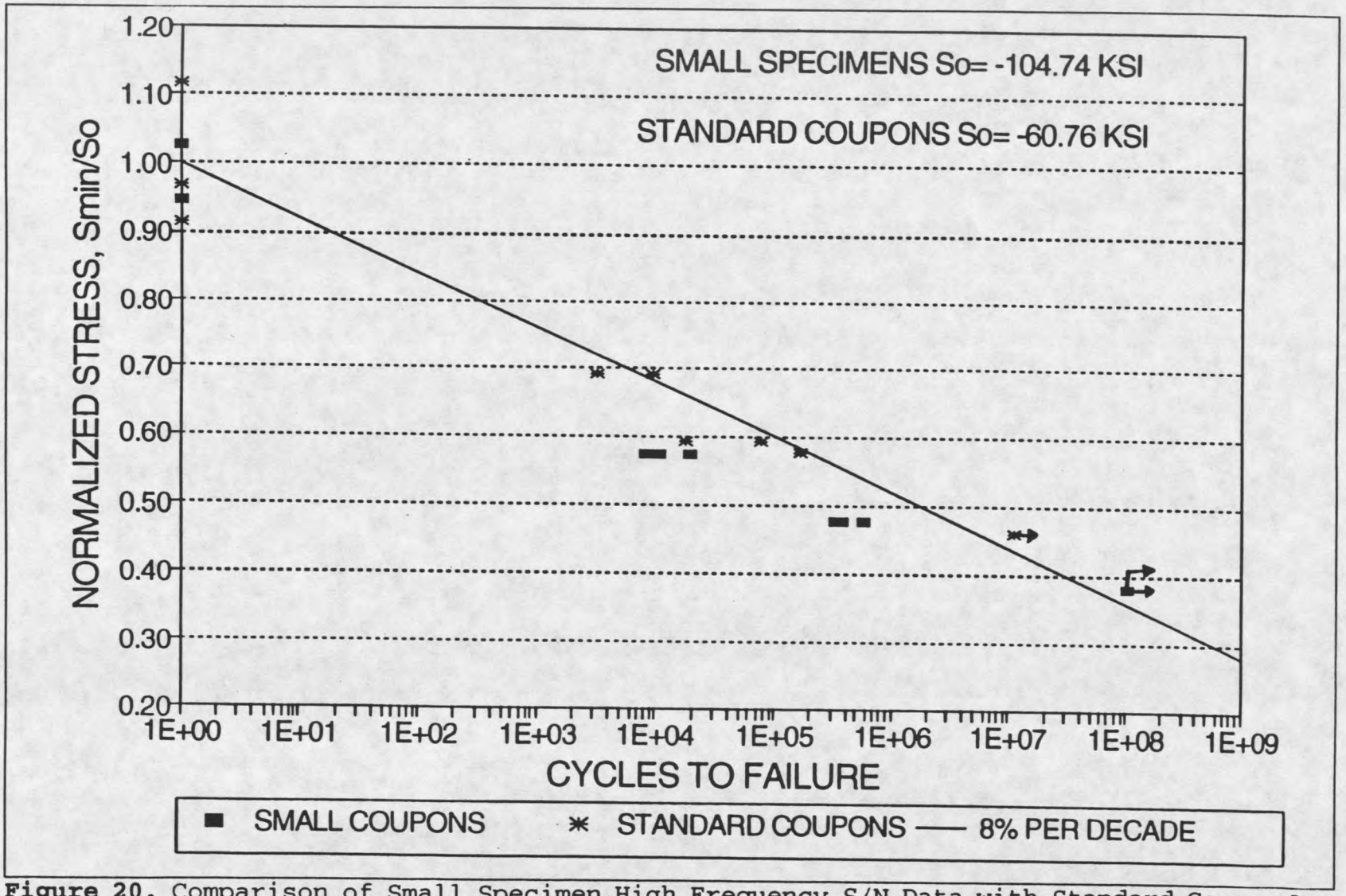


Figure 20. Comparison of Small Specimen High Frequency S/N Data with Standard Coupon Low Frequency Data.

sized coupons used by Combs are unknown, but a similar observation was made by Creed [3] for tensile fatigue of small specimens at high frequency. It could be a manifestation of unidirectional material which tend to split longitudinally in compression fatigue compared to delamination buckling observed in coupons with transverse and off-axis plies. Failure modes will be described in more detail later. Reference 34 suggests that a curvature below the linear trend is an indication of hysteretic heating problems. In this research, however, there was no indication that hysteretic heating was a problem. Measurements made with Omega Tempilaq paint clearly showed that specimen surface temperatures never rose above 100°F. It is probable that surface temperatures were below this value, but 100°F was the lowest temperature paint available.

Examination of Figure 19 also indicates that above 10^5 cycles the S/N curve is flattening out. If the power law fit for the entire data set is used to predict fatigue lifetimes past 10^8 cycles, the values would be skewed low. This is because this curve fit is influenced more strongly by low cycle data points which occur at higher stresses. If a least squares power law curve fit is done for points above 10^5 cycles (including runouts), the goodness of fit increases from R^2=0.9938 to 0.9976 (Figure 21). Furthermore, at 10^9 cycles the extrapolated failure stress rises from 31.6% of the UCS to 34.9% of the UCS, and the corresponding strain increases from 0.64% to 0.71%. This fact is very important when considering

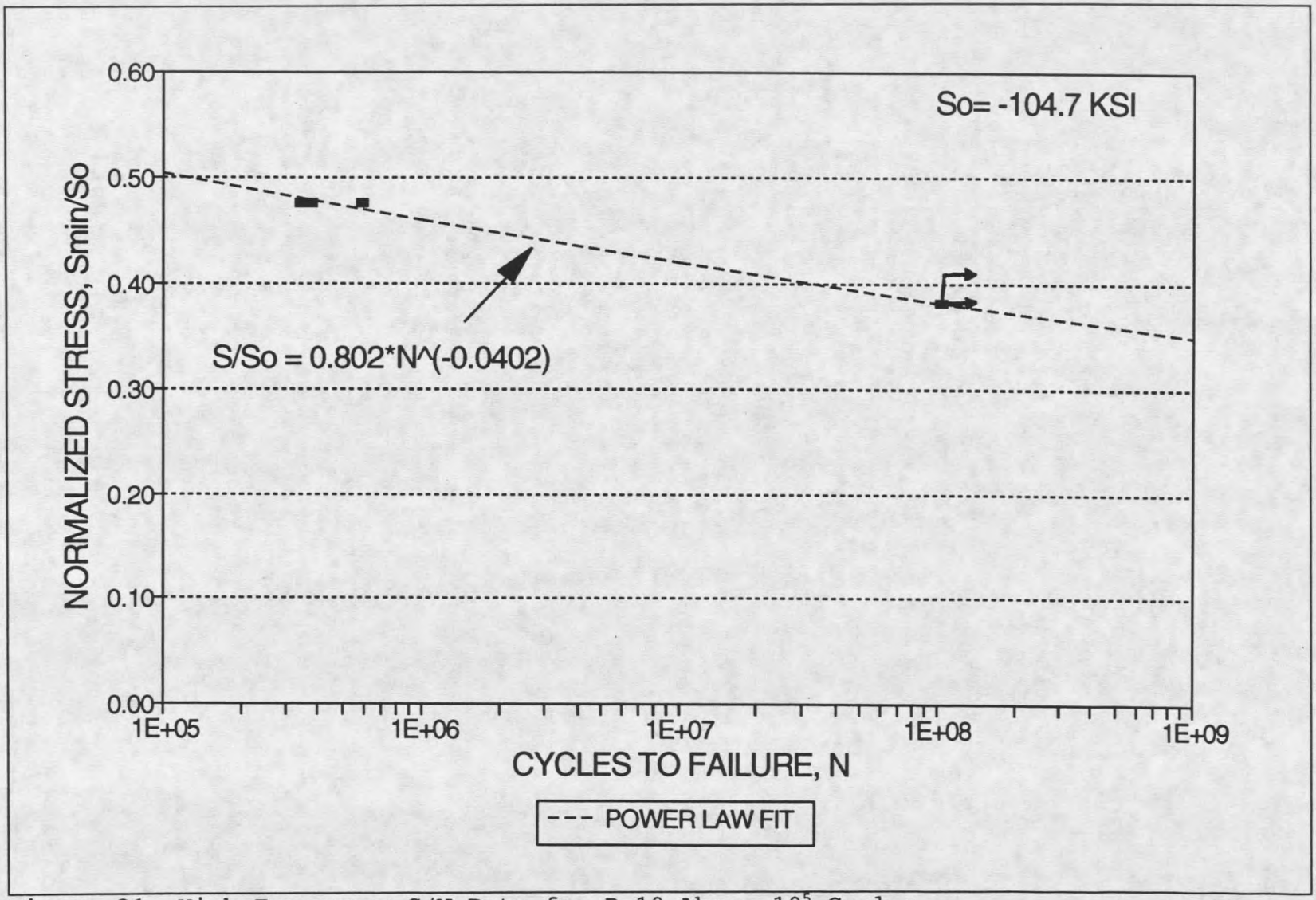


Figure 21. High Frequency S/N Data for R=10 Above 10^5 Cycles.

the design of wind turbine blades. Previously, fatigue lifetime predictions have been made using trend lines developed with low to moderate cycle fatigue data. The result is that predicted design failure loads are too low at high cycles. For engineers, this potentially means blade designs would have to be altered in order to handle the higher projected loads. This is assuming, however, that the dominant fatigue loading is caused by an event which the blade would experience for 10^8 to 10^9 cycles, such as bending caused by passing the tower each rotation. Recent studies on wind turbine service loads [2] indicate that other high stress/ low to moderate cycle conditions may actually be the dominant loading over the lifetime of a blade.

Tests were also conducted with an R value of two. The R values between ten and two correspond to the stress ratio range where most compressive loads occur in wind energy turbine blades [40]. Figure 22 shows the R=2 curve, with the raw data in Table 2. Three specimens were discarded from the S/N data set and do not appear in either Figure 22 or Table 2. Two were excluded because they slipped in the grips, producing erroneous failure cycles. The third was excluded because of tab debonding problems which resulted from trying to test the specimen at too high a percentage of the ultimate compressive strength. A power law curve also provided the best fit to the R=2 data, with a correlation of 0.923. The S/N curve slope in Figure 22 is considerably flatter than the 8% per decade

Table 2. Data for R=2 S/N Curve.

Minimum Stress (ksi)	Test Frequency (Hz)	Initial Peak Strain (%)	Cycles to Failure
-107.6	30,487 lbs/sec	-2.09	1
-107.5	30,457 lbs/sec	-2.09	1
-99.1	28,083 lbs/sec	-1.93	1
-80	60	-1.56	9255
-80	60	-1.56	12,319
-80	60	-1.56	22,071
-80	60	-1.56	46,085
-70	80	-1.36	11,347
-70	80	-1.36	38,158
-70	80	-1.36	45,312
-70	80	-1.36	103,970
-65	100	-1.26	17,937
-65	100	-1.26	3,891,657
-65	100	-1.26	1E+08 *
-60	100	-1.17	1.07E+08 *

* signifies a run-out (no failure)

observed at R=10. They follow roughly a 5.5% per decade line (R^2=0.920). This is due to the lower R value which effectively decreases the cyclic amplitude at the same minimum stress value. Specimens tested with lower amplitudes at the same minimum stress will tend to last longer than those tested with larger amplitudes at the same minimum stress level. Figure 23 compares the R=2 and R=10 S/N curves.

The region between 60 and 70% of UCS at R=2 shows some interesting behavior. The points at 66% of UCS are almost

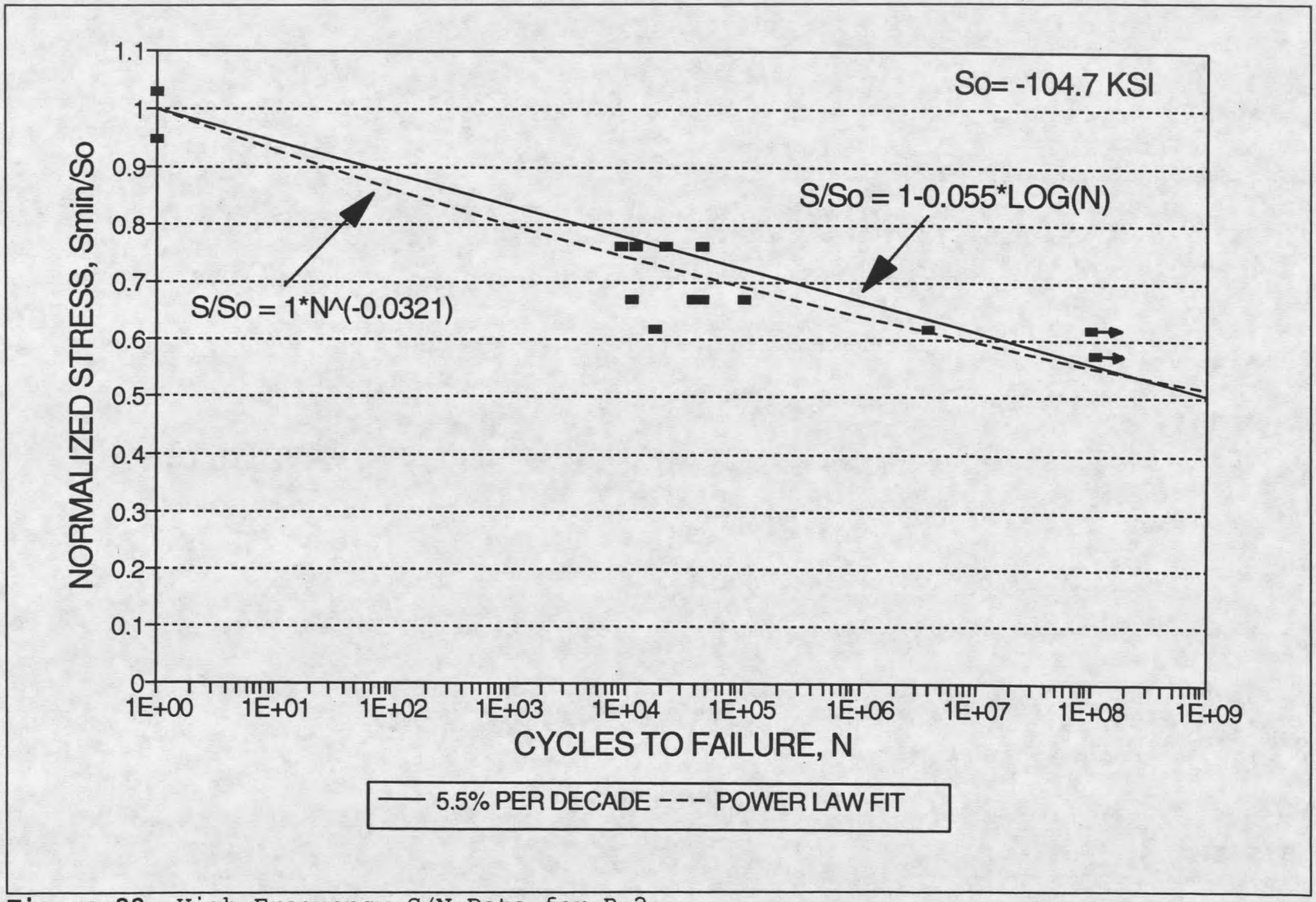


Figure 22. High Frequency S/N Data for R=2.

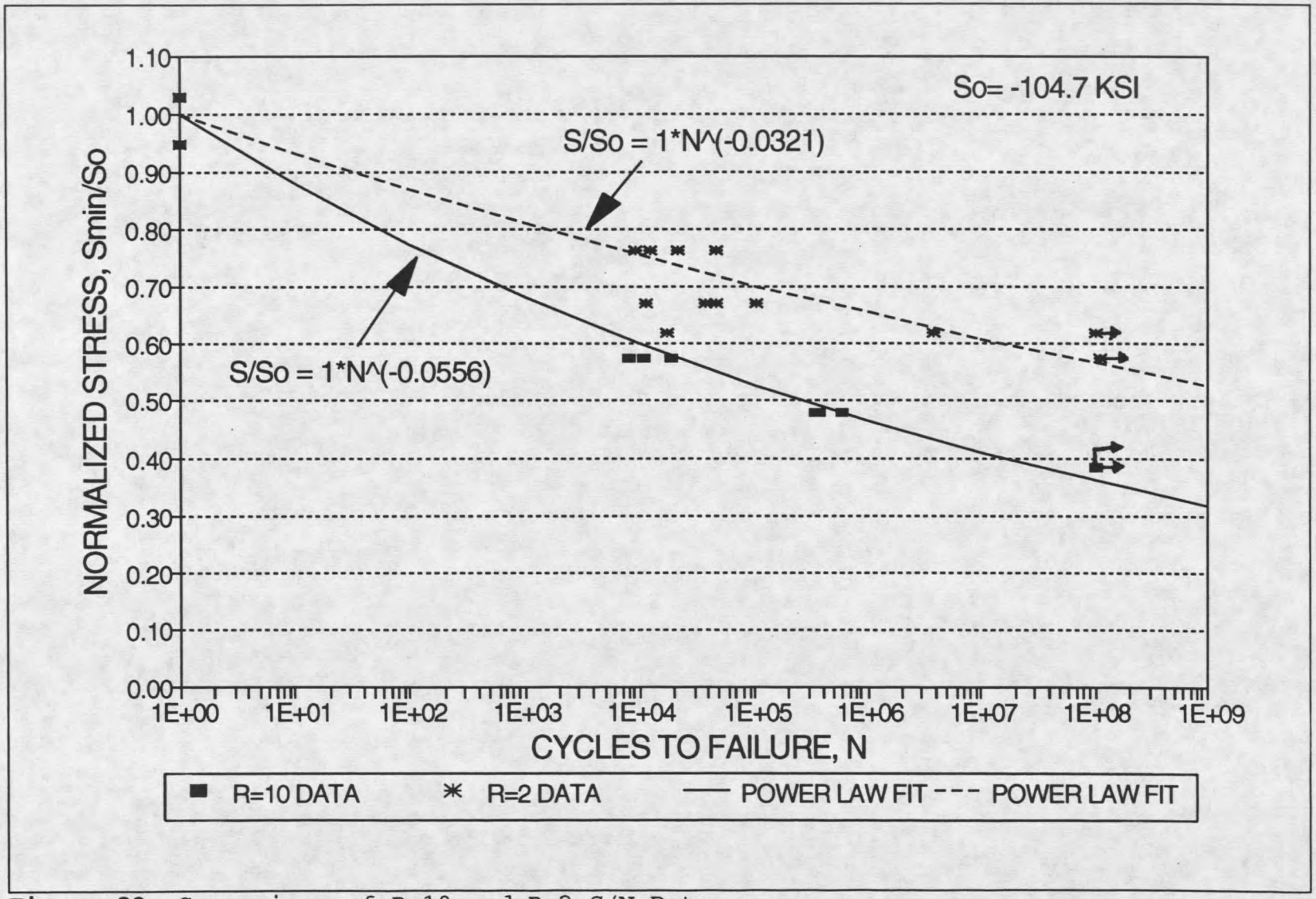


Figure 23. Comparison of R=10 and R=2 S/N Data.

directly below those at 76% UCS. This could simply be the result of a larger vertical scatterband than is present in the R=10 curve. It is also possible that this clustering, combined with the large horizontal scatter of points at 66% UCS, indicates that the slope of the S/N curve is flattening out and reaching some form of fatigue limit similar to what exists in steel. This is purely conjecture, however, and more extensive testing would be required before the presence of a fatigue limit could be confirmed.

If the high cycle (above 10^5) data are analyzed separately, the goodness of fit for a least squares power law fit actually goes down from 0.923 to 0.849 (see Figure 24). This is most likely the result of such a small data set (four points) and the strong influence exerted by the two 10^8 cycle data points which are separated vertically by only 5% of the UCS. Despite a decreased goodness of fit, the curve can still be used to examine and predict specimen high cycle behavior. The result is once again an increase in the predicted failure stress at 10^9 cycles from 51.4% of the UCS to 57.3% of the UCS, with the corresponding strain rising from 1.05% to 1.17%.

Effect of Fiber Content Variations on S/N Curves

It was observed that variations existed between the fiber volume fraction measured for the composite plate and those measured for individual specimens cut from the plate. The cause of these differences was the variable stacking pattern of the fiber bundles. The two observed packing arrangements

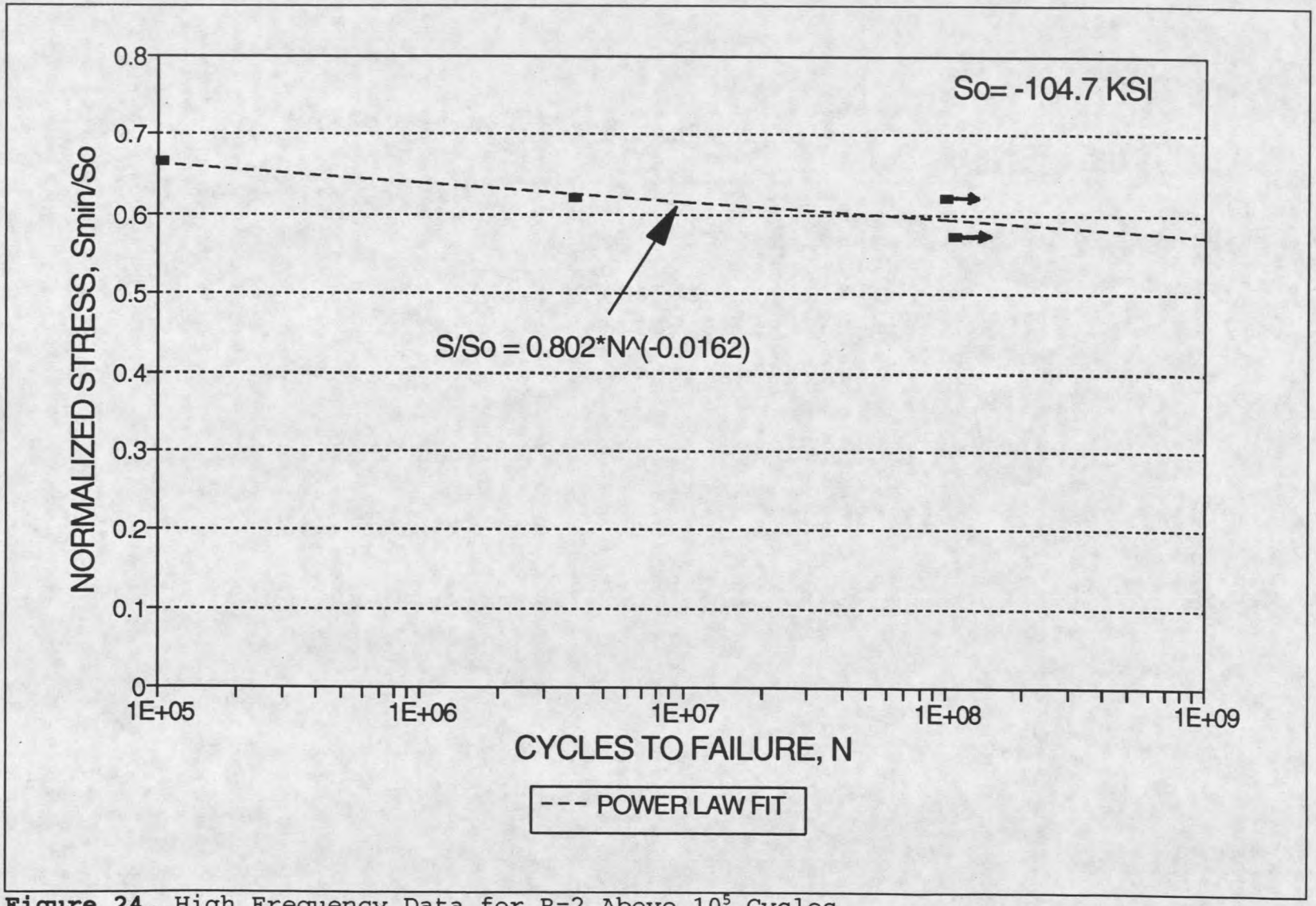


Figure 24. High Frequency Data for R=2 Above 10^5 Cycles.

Table 3. Fiber Volume Fraction Data for R=10 Curve.

Specimen Number	Minimum Stress (ksi)	Number of Fiber Bundles	% Fiber Volume Fraction	Stress/ Fiber Fraction
AC7	-50	6.25	49.74	-100.52
AC8	-60	9	61.13	-98.15
AC10	-40	6.5	51.11	-78.26
AC11	-60	6.25	48.26	-124.33
AC12	-60	6.25	48.26	-122.82
AC13	-99.1	6	45.00	-220.00
AC14	-107.6	7.5	57.24	-187.98
AC15	-50	7	60.54	-82.59
AC16	-50	6.5	45.83	-109.1
AC17	-107.5	6	45.79	-234.77
AC30	-40	7	48.05	-83.25

are illustrated in Figure 25. The inconsistent bundle arrangements made it nearly impossible for specimens to be cut with the same number of bundles across their widths. Furthermore, bundles were often cut into fractional parts. An analysis was undertaken to determine if the varying fiber contents affected the fatigue curve results. Tables 3 and 4 contain the fiber volume fractions for each specimen in the R=10 and R=2 data sets. In both cases it can be seen that the fiber volume fractions hover close to 50%. The R=10 curve has three specimens that are closer to 60%, but otherwise there are no significant variations in the fiber contents. The minimum testing stress of each specimen is normalized by fiber

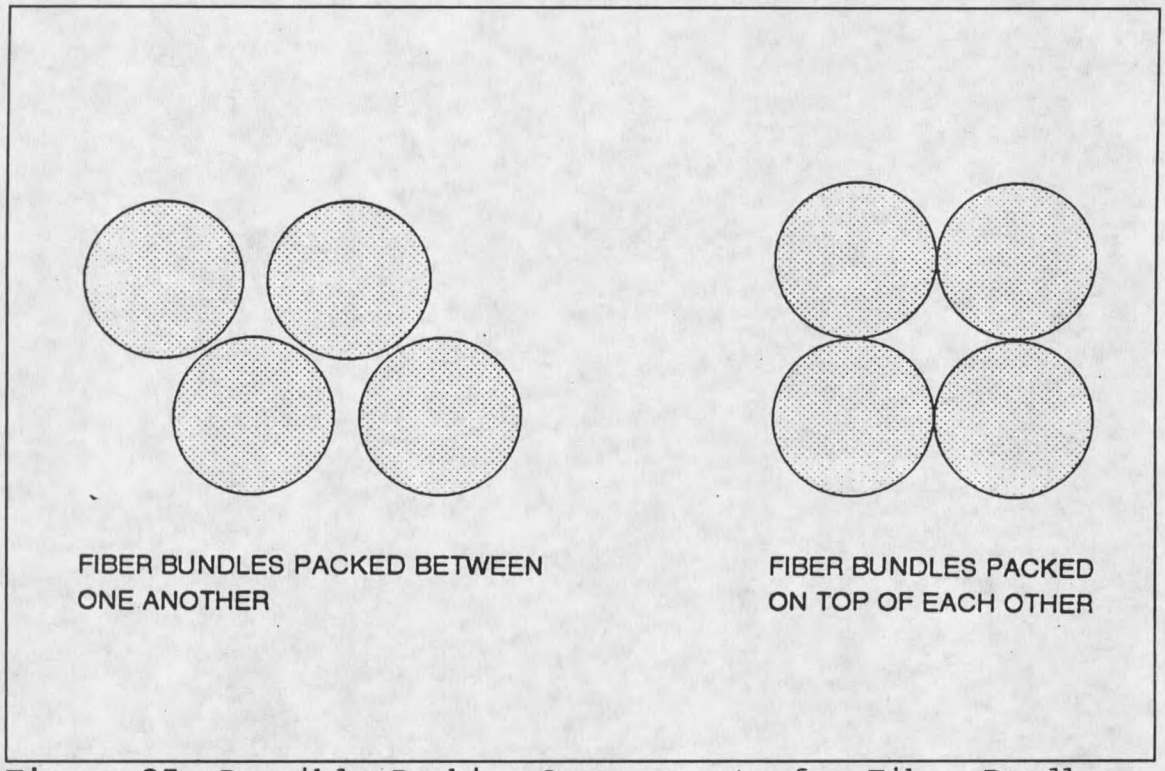


Figure 25. Possible Packing Arrangements for Fiber Bundles.

volume fraction in order to study the effects of fiber content on the S/N curves. Data from Tables 3 and 4 in the right column of both tables are then normalized to the fiber normalized S_o in order to compare them with the data from Tables 1 and 2 which do not take fiber volume fraction into account. Both the R=10 and the R=2 curves show very little difference when fiber content is taken into account. On the R=10 curve there are three points which appear to be separated from the rest of the data. These points represent the specimens with the highest fiber contents. While it does appear that these three points tend to define a curve that is below the curve defined by the lower fiber content specimens, more data are required to clarify this question. Generally,

Table 4. Fiber Volume Fraction Data for R=2 Curve.

Specimen Number	Minimum Stress (ksi)	Number of Bundles	% Fiber Volume Fraction	Stress/ Fiber Fraction
AC19	-80	6	48.96	-163.40
AC20	-80	6.5	51.11	-156.52
AC21	-70	6.25	46.87	-149.35
AC22	-70	6	45.79	-152.87
AC23	-60	6.5	49.60	-120.97
AC24	-70	6.5	52.38	-133.64
AC25	-65	6.5	48.46	-134.13
AC26	-80	6	48.96	-163.40
AC29	-80	6.5	49.31	-162.24
AC31	-70	6	44.23	-158.26
AC32	-65	6	46.06	-141.12
AC35	-65	5.75	47.51	-136.81

no consistent improvement in the S/N trends is provided by normalizing for individual specimen fiber content.

Tension

Figure 28 shows the S/N curve for an R value of 0.1, with the raw data in Table 5. The data approximately follow a 10% decrease in stress to produce a decade greater lifetime which has been observed in the literature [7]. The points out to 10^8 represent the first known published data out to this cycle range for well aligned unidirectional composites. Testing time for these points was again on the order of 11 days.

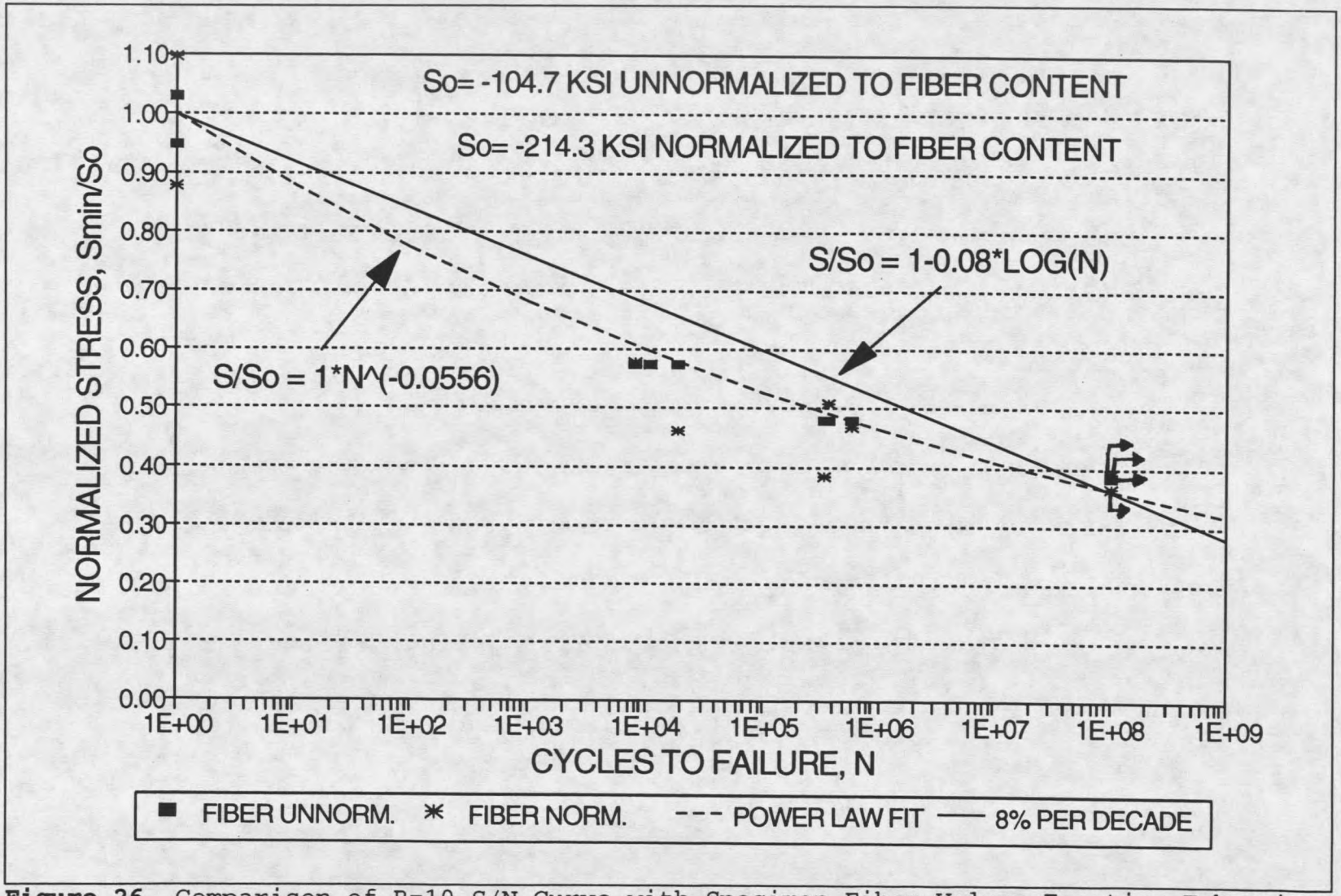


Figure 26. Comparison of R=10 S/N Curve with Specimen Fiber Volume Fraction Taken into Account and Ignored (power law fit is to data not normalized by fiber content).

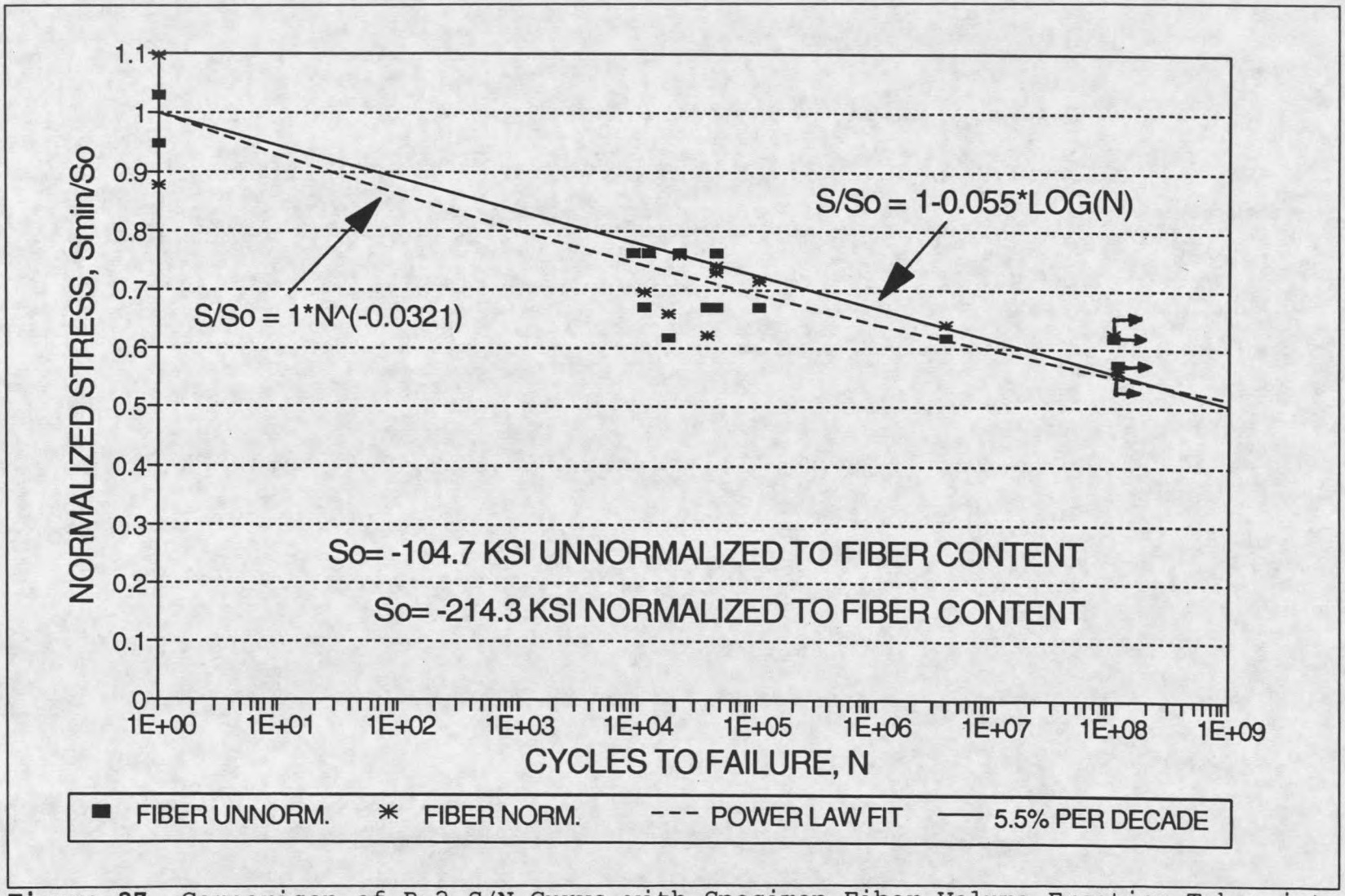


Figure 27. Comparison of R=2 S/N Curve with Specimen Fiber Volume Fraction Taken into Account and Ignored (power law fit is to data not normalized by fiber content).

Table 5. Data for R=0.1 S/N Curve.

Maximum Stress (ksi)	Test Frequency (Hz)	Initial Peak Strain (%)	Cycles to Failure
236	23,970 lbs/sec	3.53	1
220	34,467 lbs/sec	3.28	1
202	31,667 lbs/sec	3.01	1
195	28,316 lbs/sec	2.91	1
100	20	1.49	2982
100	20	1.49	45,845
68	60	1.01	157,502
68	60	1.01	702,844
60	80	0.896	602,984
60	80	0.896	2,269,945
45	100	0.672	5,902,329
45	100	0.672	78,810,903 *
45	100	0.672	1.11E+08 *

* signifies a runout (no failure)

The curvature below the 10% per decade line is similar to that observed in both Creed's [3] research (Figure 30) and in compression as discussed earlier. Near 20% of the ultimate tensile strength (UTS) there is increased scatter indicating a possible fatigue limit. As with the R=2 curve, however, there is not enough data to draw a solid conclusion. The static strength values found in Table 5 are unusually high. Typical unidirectional E-glass/ epoxy prepreg (50% fiber content) has a UTS of 160 ksi [41]. This difference is most likely the result of an increased fiber volume fraction caused

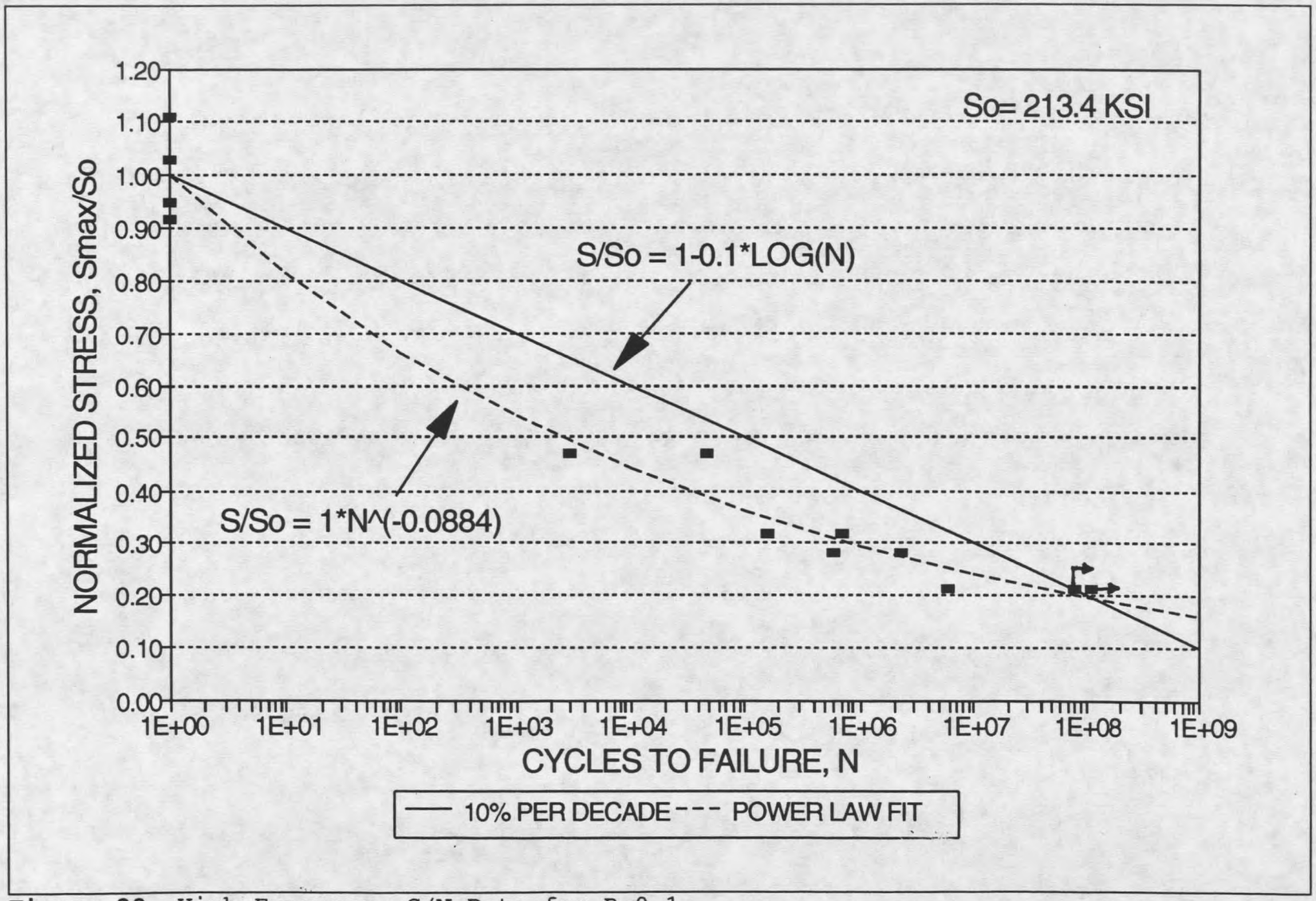


Figure 28. High Frequency S/N Data for R=0.1.

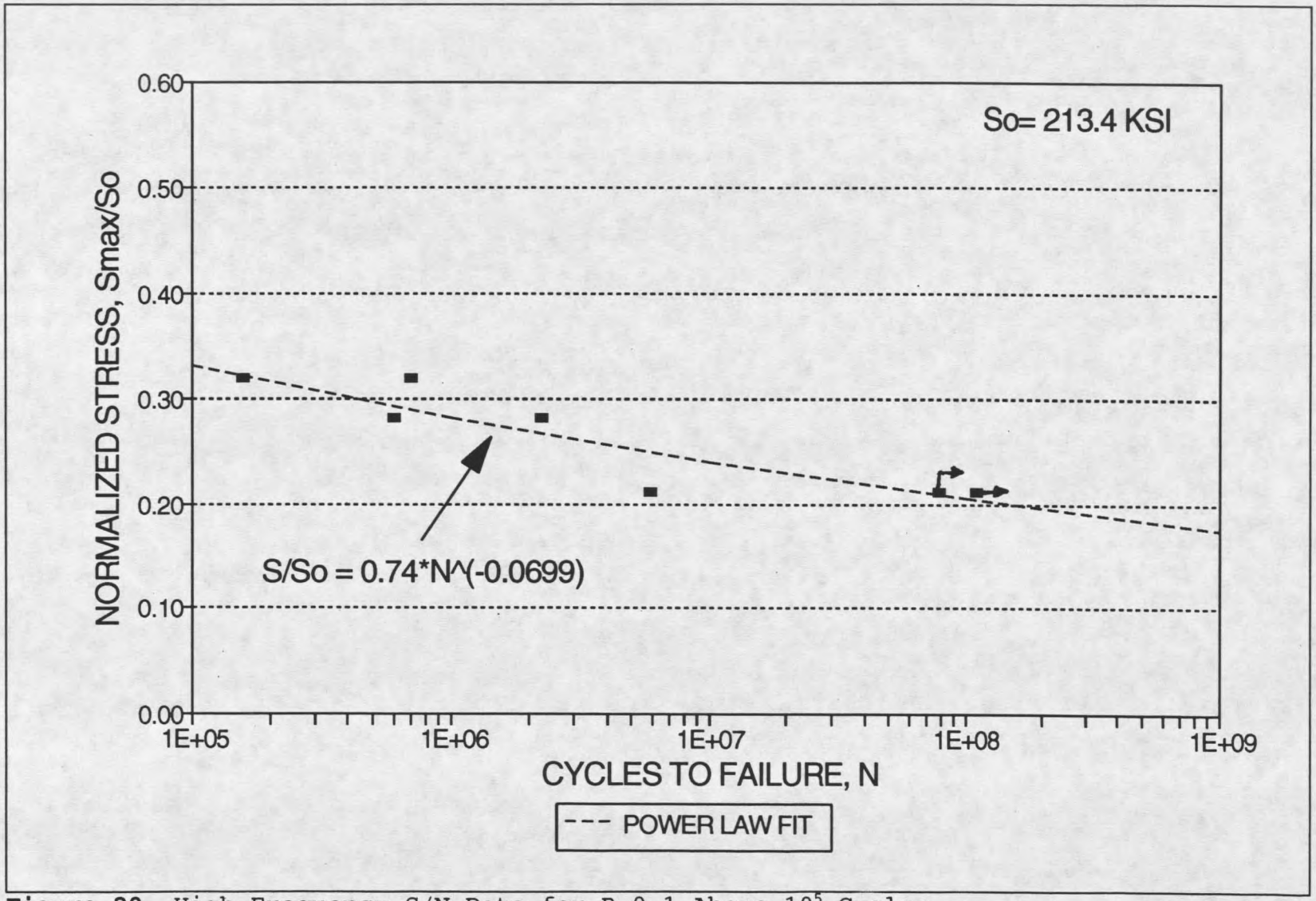


Figure 29. High Frequency S/N Data for R=0.1 Above 10^5 Cycles.

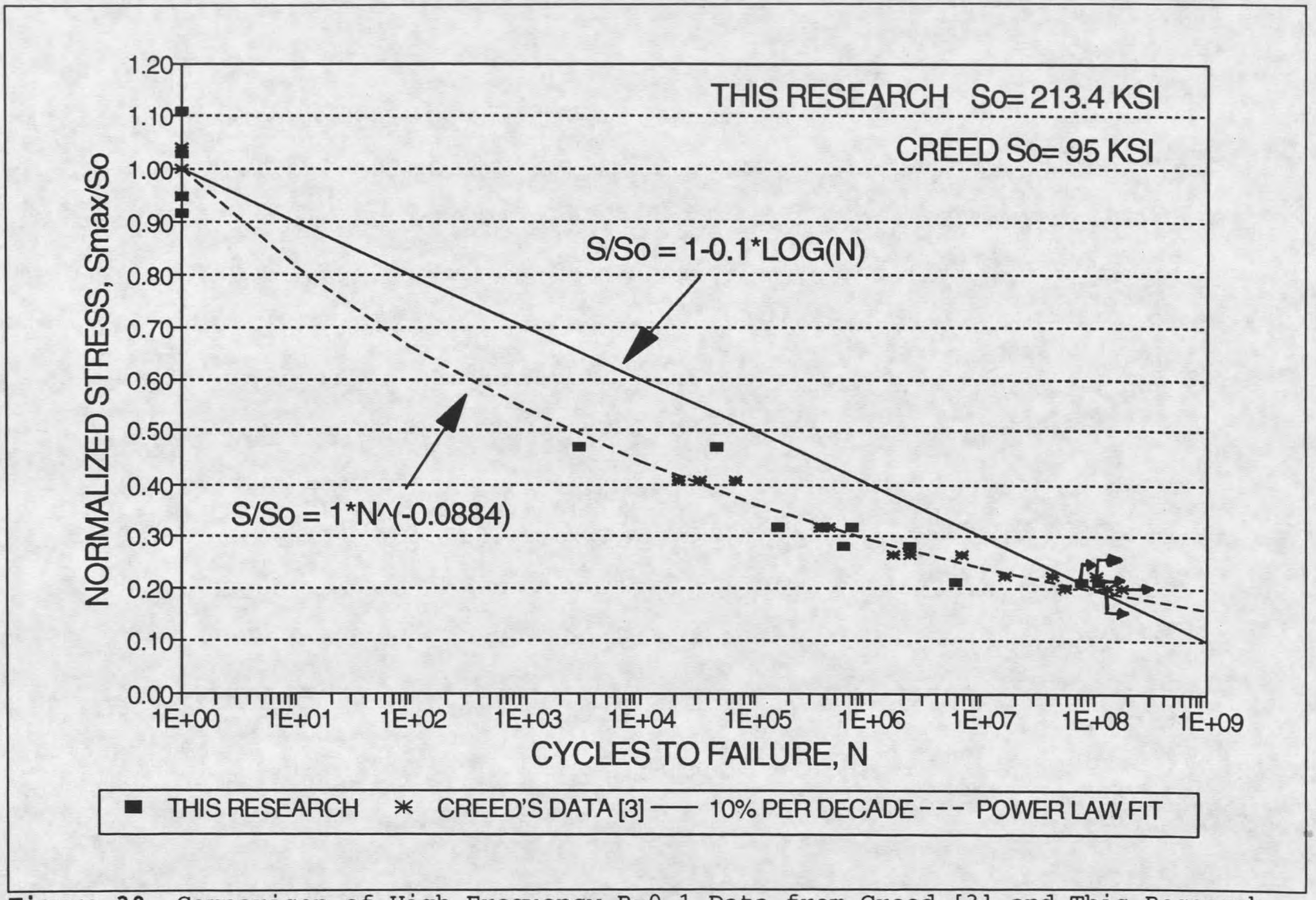


Figure 30. Comparison of High Frequency R=0.1 Data from Creed [3] and This Research.

by the tapering process described earlier.

A power law curve fit (including runouts) described the data best (R^2=0.9877). At higher cycles the S/N curve appears to be flattening out. When only high cycle (above 10^5 cycles) data were curve fit (runouts included), the goodness of fit actually drops, however, to 0.8987 (see Figure 29). The reason for this is most likely the high degree of horizontal scatter present. The high cycle curve fit is still useful, though, in illustrating the observation made with the compression S/N curves, that the extrapolated failure stress at 10^9 cycles increases compared with the failure stress projected by the curve fit using the entire data set. In this case the projected failure stress rises from 16% of the UTS to 17.4% of the UTS, and the strain rises from 0.51% to 0.55%. Compared with Creed's results [3] the strain to produce 10^8 cycles runouts is now increased to about 0.67% compared with 0.40% for the poorly aligned material. Figure 30 compares the data obtained by Creed [3] and the data obtained in this research. The curves have a high degree of correlation, despite the differences in material used, and measured static strengths. Therefore, it is possible to predict the behavior of a second material with a different static strength from the results in this thesis for strong, well aligned material by using normalized S/N curves.

Failure Modes

Specimen failures occurred catastrophically in the gage section, without any noticeable warning such as preliminary cracking or delamination. The predominant failure mode was shear crippling. Specimen failure modes are somewhat different than those observed by Combs [39] (Figure 31) for larger coupons and those in the literature [35] (Figure 32).. The larger coupons in these studies tended to experience more delamination/ buckling of the outside plies, while some inner plies experienced shear crippling. The greater degree of delamination/ buckling observed in the larger coupons may be

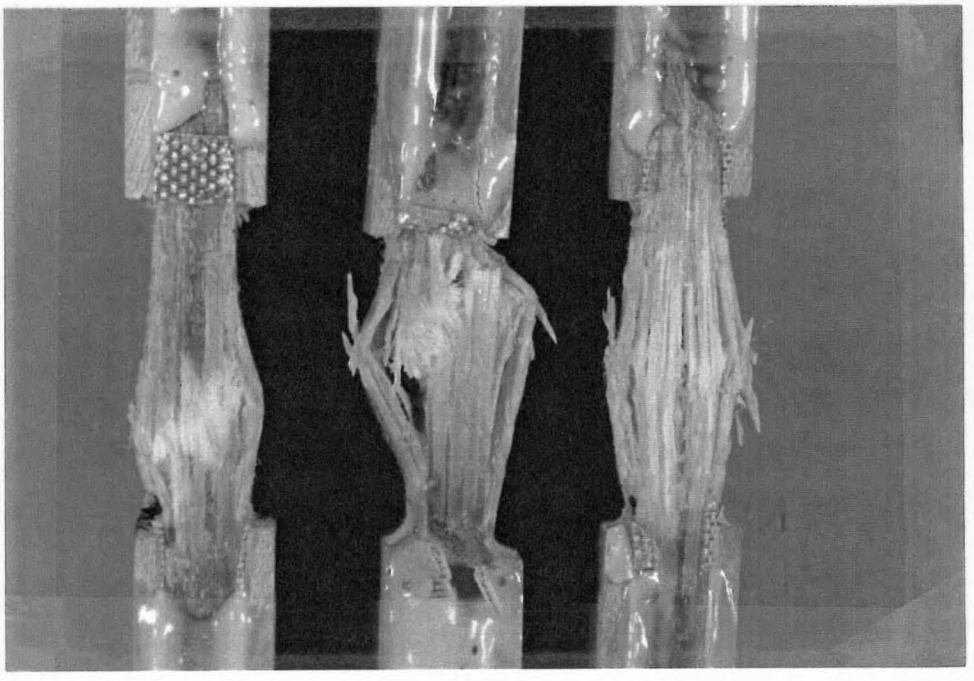


Figure 31. Failure Modes Observed by Combs [39].

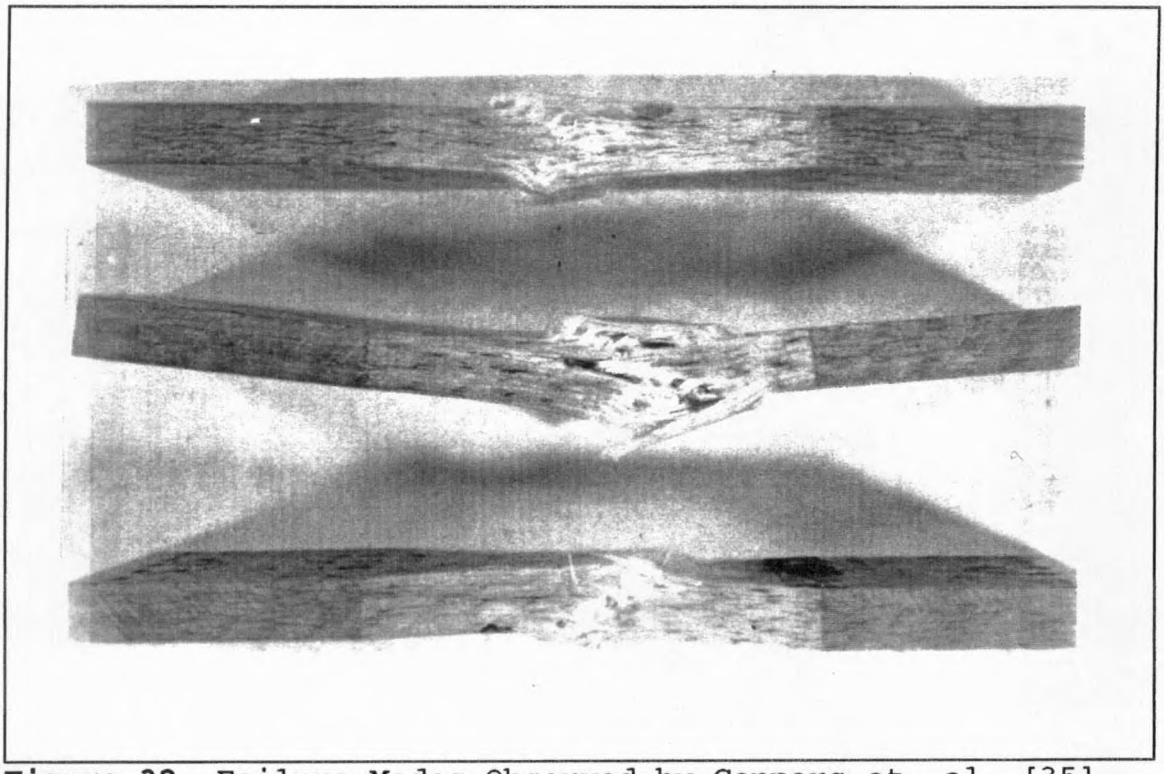


Figure 32. Failure Modes Observed by Conners et. al. [35].

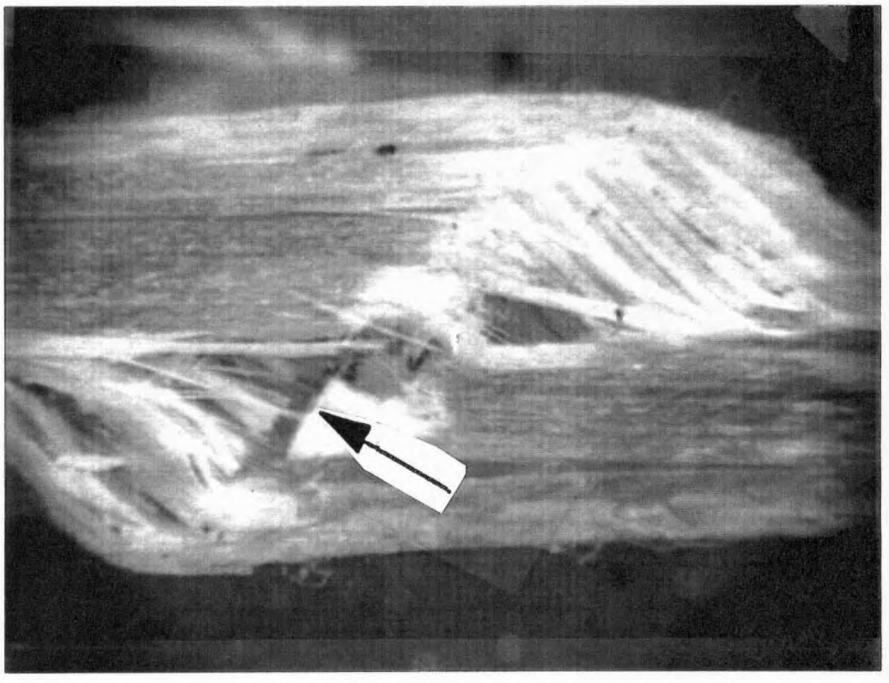


Figure 33. Failure Mode of Inner Plies of Specimens Used by Combs [39].



Figure 34. Failure Modes Observed in this Research.

the result of transverse and off-axis plies being present. Furthermore, the thickness of the specimen may have an effect on failure mode. Since the small high frequency specimens have only two plies, there are no outside plies to delaminate. Therefore, the high frequency specimen failure mode appears to be more representative of the failure modes observed primarily in the interior plies of the larger coupons (see Figure 33). Figures 34-36 show the failure modes observed in this research.

The difference in the failure modes between small and large coupons does not appear to be critical. The S/N data demonstrate that the smaller volume of material found in the high frequency specimens behaved in a similar manner to the larger volumes found in standard size coupons. This is an indication that the data obtained from high frequency tests conducted on small volumes of material may be used to predict

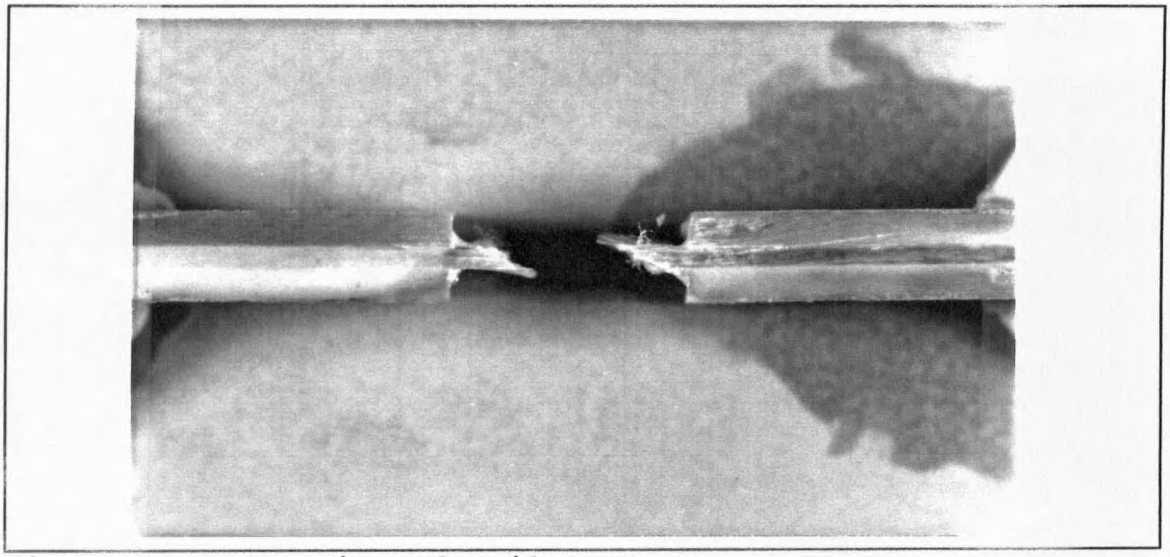


Figure 35. Edge View of Failure Zone.

the behavior of larger volumes of material found in coupons and structures. In fact, all of these modes appear to be matrix dominated, and the fatigue sensitivity is similar to that reported for neat matrix materials [30].

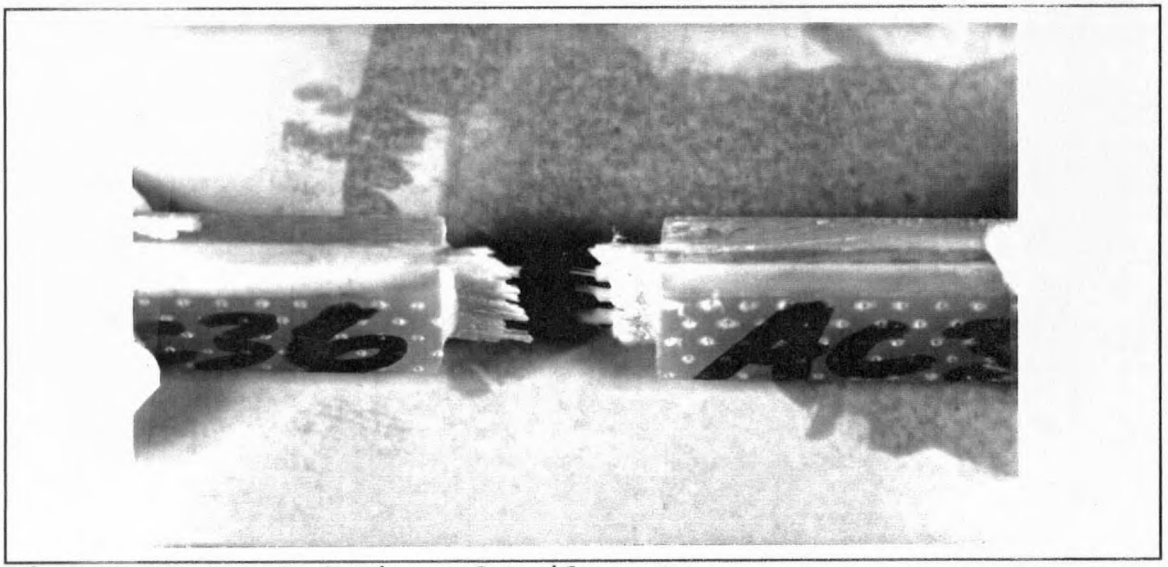


Figure 36. Angled View of Failure Zone.

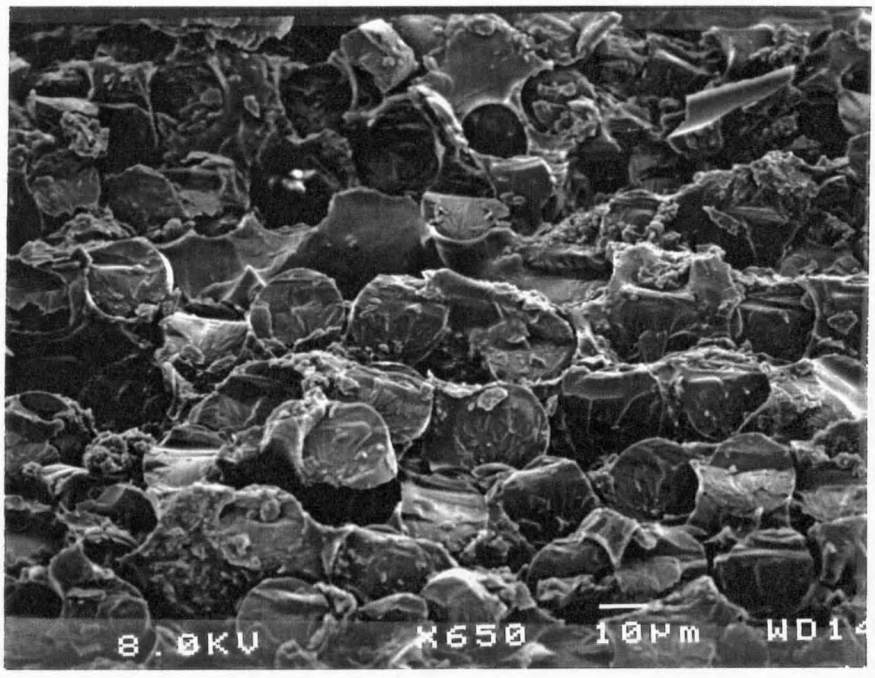


Figure 37. Fracture Surface of Static Specimen (AC14).

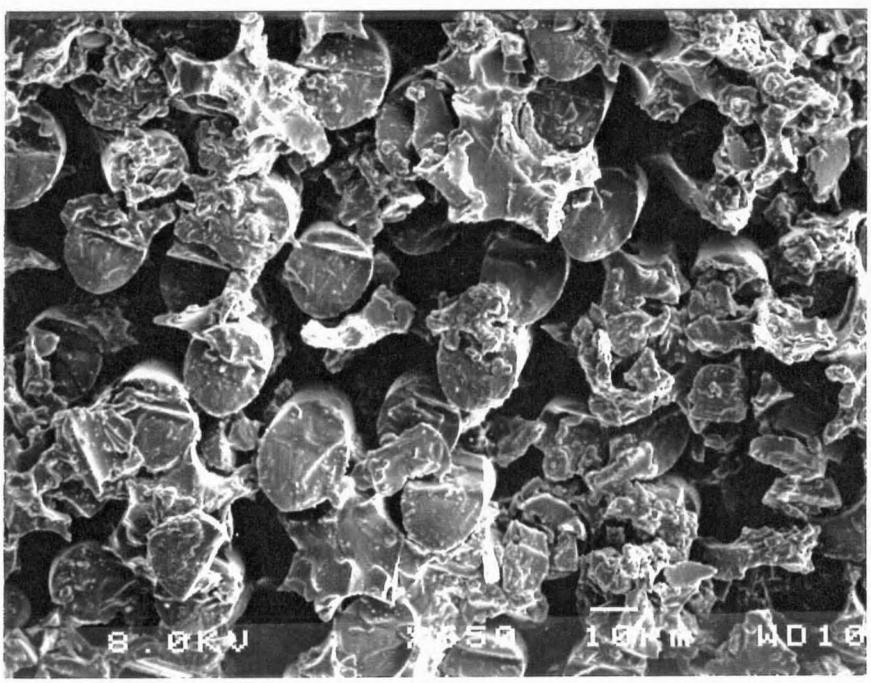


Figure 38. Low Stress Fatigue Fracture Surface (AC15).

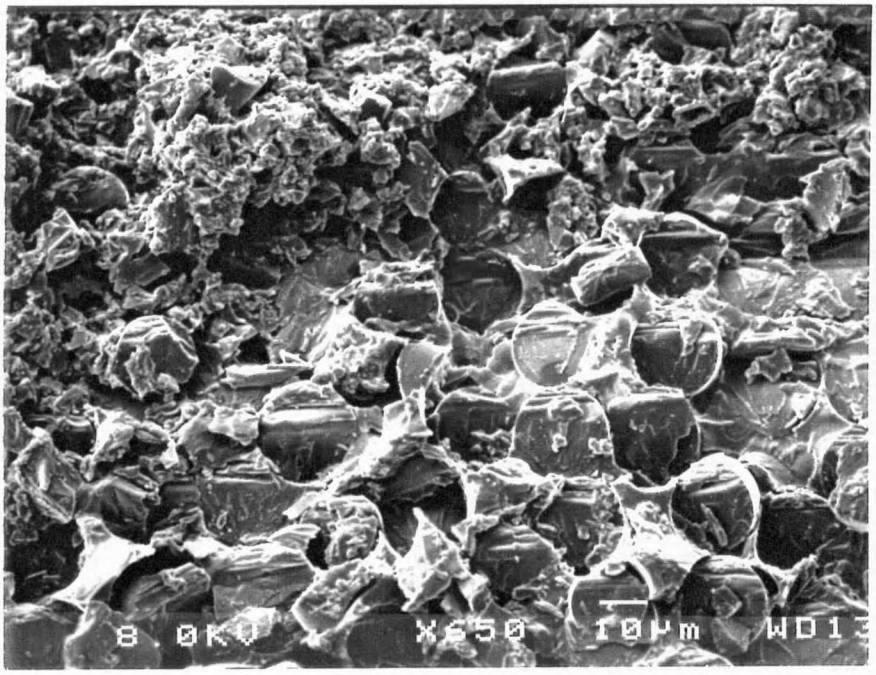


Figure 39. High Stress Fatigue Fracture Surface (AC8).

Figures 37-39 show SEM photographs of representative fracture surfaces of static and fatigue specimens. It can be seen that while the overall fracture surface is a flat fracture plane oriented at about 45° to the load, the individual fibers broke from microbuckling, which is apparent because of the two tiered fracture surfaces of each separate fiber. This indicates tensile failure on one half and compressive failure on the other [42]. The depressed half of the fiber is the tensile failure region, while the raised half is the compression failure region. These failures occurred in a very narrow band about 45° to the load axis in the thickness direction (Figures 35 and 36).

Frequency Effects

The results in Figure 20 (page 49) suggest that the higher frequency data show a slightly shorter lifetime than do standard coupons tested at 10-20 Hz. This may be the result of other differences in size and ply configuration, but frequency effects were further examined using small specimens tested at the same stress level but with varying frequency (10, 30, and 50 Hz); the relatively high stress of -55 ksi was required to obtain reasonable test durations at 10 Hz. Table 6 compares the data from these tests. The data do show a frequency dependence for the number of cycles to failure, with longer lifetimes for some of the 10 Hz specimens. However, the magnitude of the effect does not appear to be great when the data for 50 and 60 ksi are taken into account from Table 1. The differences in stress between 60 and 55 ksi and 50 and 55 ksi are small, and the vertical scatter bands for these three stress levels may very well overlap, similar to the scatter of 8.5 ksi in the one-cycle results. This could lead to an overlapping of specimen lifetimes. Therefore, the frequency effect is moderate at most, and more extensive data taken at several more widely varying stress levels would be required before a solid conclusion could be reached as to whether the data observed in Table 6 illustrate a frequency

dependence. The data at 30 and 50 Hz appear to correlate closely, while those at 10 Hz have a longer average lifetime.

Table 6. Frequency Effects (R=10).

Minimum Stress (ksi)	Test Frequency (Hz)	Cycles to Failure
-55	10	4021
-55	10	496,974
-55	10	1,336,317
-55	10	3,638,153 *
-55	30	6550
-55	30	10,192
-55	50	4765
-55	50	8349
-55	50	12,660

* signifies a run-out (no failure)

An exhaustive data collection program was not undertaken in this thesis because of the time required to test specimens to high cycles at 10 Hz. The need for data at this extreme originates from the fact that the S/N curve slope for compressive data is low. This means that in order to avoid stress levels where vertical scatter bands could overlap, specimens would have to be tested in the very low cycle to failure range and the very high cycle to failure range.

A possible cause of shorter lifetimes at high frequency lies in differences in the load waveforms. Figure 40 shows the unfiltered waveforms obtained for 10 and 100 Hz. Time has been normalized (t/t_o, where t_o is the time for each waveform

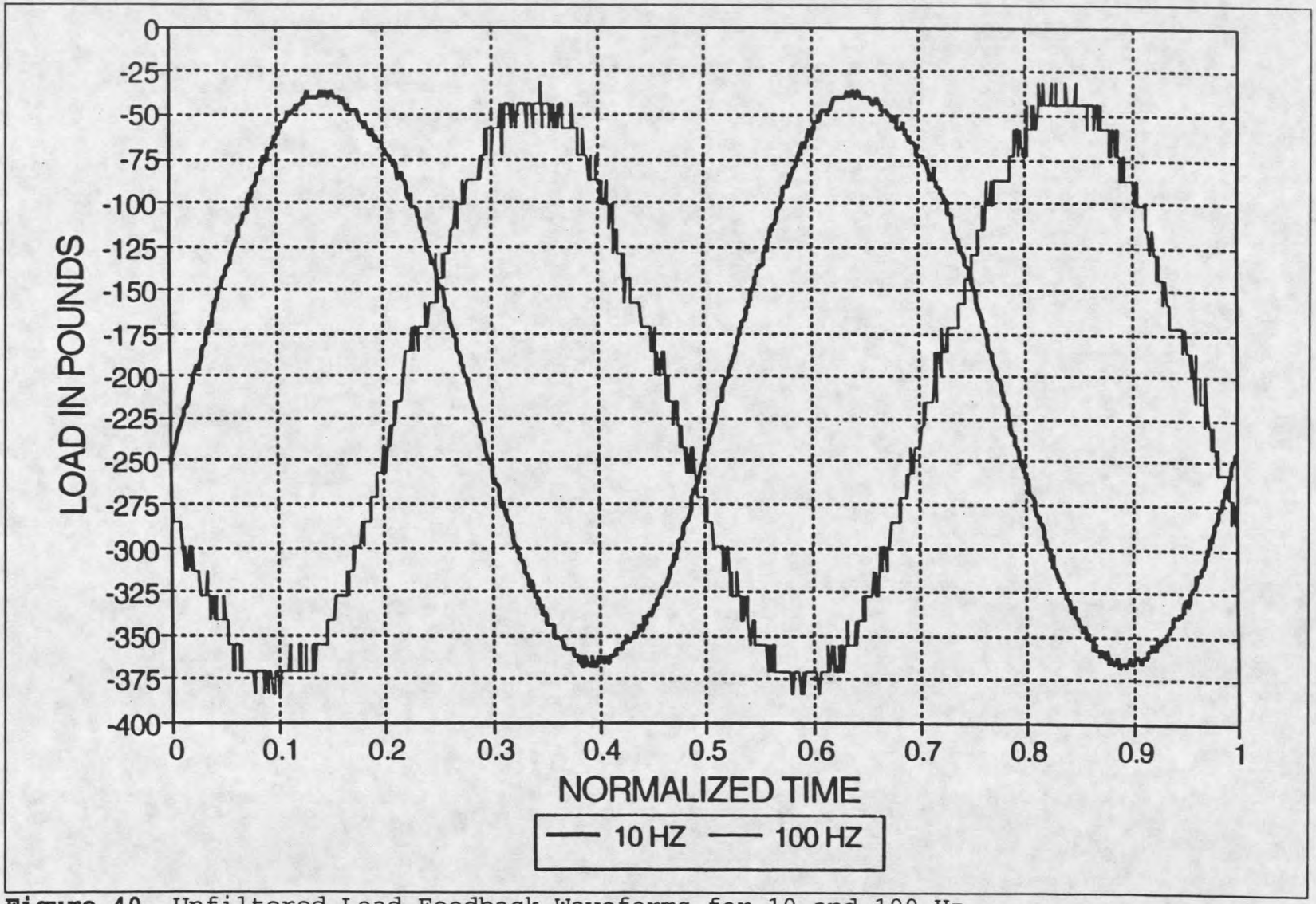


Figure 40. Unfiltered Load Feedback Waveforms for 10 and 100 Hz.

to complete roughly two periods of oscillation) so that both waveforms can be compared on the same scale. The 100 Hz waveform (as measured by the load cell) has spikes at the minimum load level which fall above and below the command sine wave minimum load level of -364 pounds. The spikes are noise, and the closed-loop load control system may try to respond to the noise. If it is possible for the machine to respond to these spikes, the actual minimum stress level being tested could be more negative than the desired minimum stress level. For Figure 38 this difference in stresses could be as large as 1650 psi which, from the slope of the S/N curve at R=10, could result in a shorter lifetime by about 13% of a decade. The spikes could also produce an added low amplitude high frequency cycling of the specimen. However, it is doubtful that the testing machine responds to the spikes.

An analysis was also performed with the data filtered because the spikes at 100 Hz were believed to be excessive electrical signal noise. The rationale for this decision was an examination of the output signals which showed that the specimen was experiencing primarily the test frequency and not sizable loads at other frequencies. Figures 41 and 42 illustrate this analysis. The breakdown plots of signal component amplitude versus frequency show that the dominant signal components are at the test frequencies of 10 and 100 Hz. The other signal components all have extremely small amplitudes compared to the test frequency component (4 to

16%), and therefore could be filtered out without adversely affecting or altering the feedback waveform data. If there had been other major amplitude components of the output signal (above 50% of the test frequency amplitude) it would have indicated that there were potential harmonic vibrations occurring in the test fixture. This would have been a major problem with the high frequency fatigue tests because the loading patterns on the specimens would have been very different from those at 10 Hz.

The filtered waveforms in Figure 43 show the load patterns that the specimen experienced during testing.

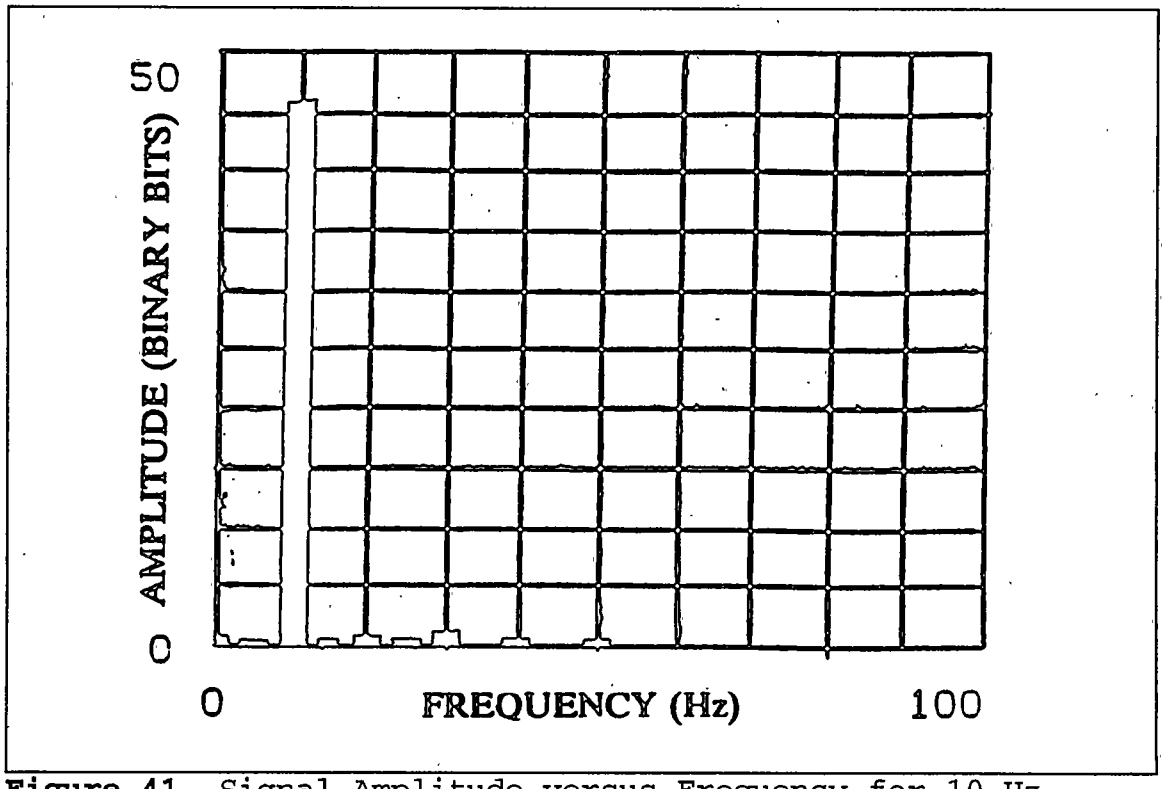


Figure 41. Signal Amplitude versus Frequency for 10 Hz.

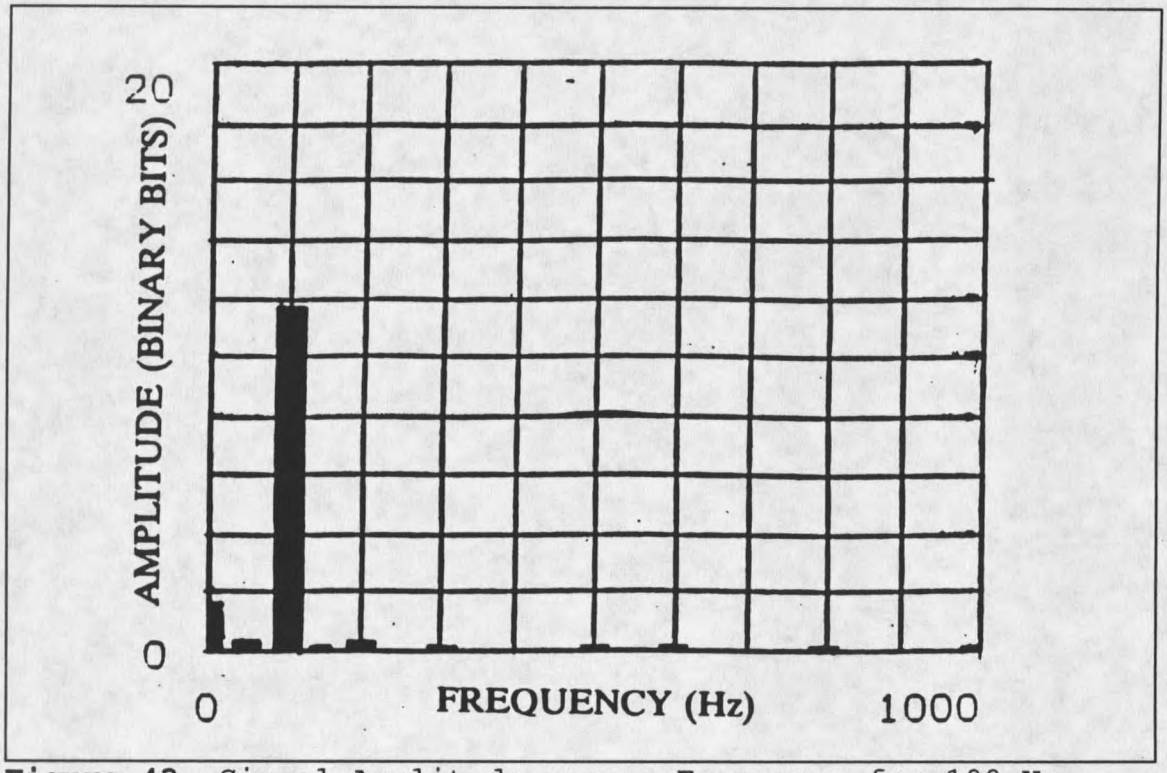


Figure 42. Signal Amplitude versus Frequency for 100 Hz.

Identical waveforms would indicate that the specimen was being tested the same at 100 Hz as at 10 Hz; the only difference being a higher loading rate at 100 Hz. As can be seen in Figure 43, both feedback curves are similar sine waves (the command signal is a sine wave). The fact that both the high and low frequency filtered waveforms are pure, undeformed sine waves is very important because it means that there were no distortions in the loading pattern caused by an increase in test frequency, assuming that the machine does not respond to the high frequency spikes noted earlier. Deformations in the 100 Hz feedback waveform would have indicated that the testing machine was unable to operate properly at such a high frequency. It would also mean that at 100 Hz the specimen is

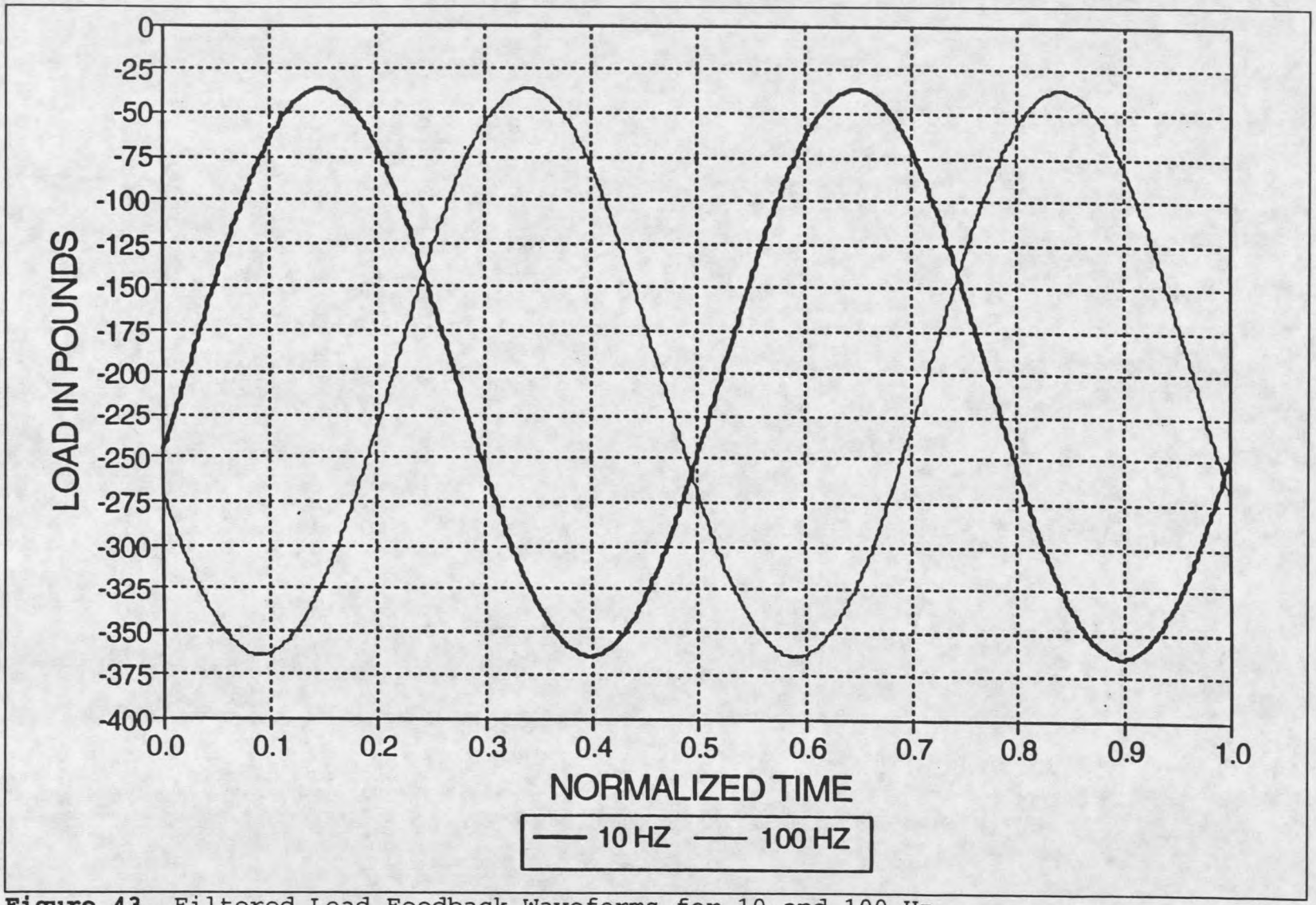


Figure 43. Filtered Load Feedback Waveforms for 10 and 100 Hz.

being cyclicly loaded differently than at 10 Hz which would most likely affect fatigue performance. It is also apparent from Figure 43 that the different sine waves oscillate between the same minimum and maximum loads, indicating that the specimen was experiencing the same loading pattern.

It is stressed, however, that while the filtered waveforms appear to be in good agreement, it is not known for certain what the spikes in the unfiltered 100 Hz waveform are measuring. If the spikes represent high frequency load application, then this might explain some of the frequency effects observed. However, if the spikes are electrical noise, the filtered waveforms illustrate the loading patterns experienced by the specimen at 10 and 100 Hz, which in this case are identical.

CHAPTER FIVE

CONCLUSIONS AND RECOMMENDATIONS

Conclusions

The objectives of this research were to develop a valid, reproducible test procedure for high frequency compressive fatigue testing and to obtain base-line fatigue data at R values of ten and two using well aligned unidirectional glass/polyester. Work was also done to expand the high frequency tensile fatigue test method developed by Creed [3] to include well aligned unidirectional material. These goals were achieved by employing the test specimen geometries shown with thin specimens which had increased heat transfer so they could be cycled at frequencies greater than those used for standard size coupons. Temperature measurements using thermal paint indicate that significant hysteretic heating did not occur.

High frequency fatigue data for an R value of ten was compared to trends in the literature and found to be in good agreement with roughly an 8% per decade decrease in strength. The data out to 10^8 cycles represent the first known published points at these lifetimes. Comparison was also made with standard coupons manufactured from the same material as the high frequency specimens and run at lower frequencies (10-20

Hz). Both sets of data were in good agreement following roughly an 8% per decade line. High frequency data points in the 10^4 to 10^5 cycle range, however, were slightly below the trends observed both in the literature and with the standard size coupons composed of materials used with the small specimens. The data were found to be described best using a least squares power law curve fit (including runouts). The reasons for this trend are unclear, but the same trend was observed by Creed [3] for high frequency tensile fatigue.

Above 10^5 cycles the slope of the high frequency S/N curve flattened, and a separate least squares curve fit of these points (including runouts) was found to have a better goodness of fit than the curve fit using the entire data set. The result of this analysis was that the extrapolated failure stress at 10^9 cycles rose from 31.6% of the UCS to 34.9% of the UCS, which is significant for design purposes.

Fatigue data obtained for an R value of two showed an S/N curve with a lower slope than the R=10 curve. The data approximately followed a 5.5% per decade decrease in strength, but was defined best with a least squares power law curve fit (including runouts). The lower slope resulted from the smaller R value which decreased the cyclic amplitude. A large cluster of points occurred between 60 and 80% of the UCS. It is hypothesized that there could be a potential fatigue limit occurring at 62% UCS because of the large horizontal scatter band observed at that stress level. However, this is

uncertain given the limited amount of data obtained at that stress level in this study. A least squares power law curve fit was done with the high cycle (above 10^5 cycles) data (including runouts) for the R=2 curve and it showed that the projected failure stress at 10^9 cycles rose from 51.4% UCS to 57.3% UCS.

The fiber volume fraction of each specimen was found to vary compared to the fiber content of the composite plate from which specimens were cut. An analysis showed that fiber volume fraction variations did not affect the S/N curves.

The data for an R value of 0.1 (tensile fatigue) showed good agreement with literature [7] and approximately followed a 10% per decade decrease in strength. The static strength values were unusually high, most likely due to an increased fiber content in the gage section as a result of the thickness tapering process. A power law curve fit (including runouts) described the data best, with the points in the medium cycle range falling slightly below the 10% per decade line. This trend was also observed both by Creed [3] for high frequency tensile fatigue and in this research with high frequency compression fatigue. Above 10^5 cycles the S/N curve flattened out, and a separate power law curve fit of these points (including runouts) showed that the projected failure stress at 10^9 cycles rose from 16% of the UTS to 17.4% of the UTS. This difference is caused by low cycle data having a greater

influence on the curve fit when the entire data set is utilized.

The small high frequency coupons were observed to have similar failure modes in compression compared to standard size coupons. This lends support to the hypothesis that high frequency data can be used to predict the behavior of coupons cycled at lower frequencies.

Frequency effects were examined by comparing small high frequency coupons tested at the same stress level with varying frequencies. The results showed that some specimens run at 10 Hz had longer lifetimes than specimens run at 30 and 50 Hz. More extensive data would be required before a solid conclusion could be drawn regarding the effect of test frequency on specimen lifetime, or its origin.

Recommendations for Further Research

This research has extended knowledge regarding high cycle fatigue behavior of unidirectional glass/ polyester composites in compression. The scope of this thesis, however, was limited. As a result, there are numerous topics for future researchers to examine.

One important question that needs to be addressed is how do other composite materials behave at high cycles. Different fibers and matrices need to be tested out to 10^8 cycles to see if high cycle behavior is material dependent. For wind turbines this means E-glass fibers combined with vinylester

and epoxy resins. Also of interest is the behavior of different layup configurations. Despite the fact that compression is matrix dominated, it is important to examine whether or not different fiber orientations behave differently at high cycles compared to low cycles.

Another area of research importance is high cycle performance of composites tested at various R values. A thorough database would allow researchers to construct a Goodman diagram (plot of mean stress versus stress amplitude) for wind turbine materials out to 10^8 cycles. This would aide engineers in wind turbine blade design. The area of most interest besides pure tension and compression fatigue is reversed loading (R=-1). As a turbine blade bends when it passes the support tower the blade surfaces may undergo a change in loading from tension to compression or vice versa. This loading cycle has been shown to be more destructive than either tension-tension or compression-compression fatigue [19], and could prove to be critical to future wind turbine blade design.

The observed frequency effects need to be more closely examined. It is critical to determine the validity of using 100 Hz fatigue data to predict the behavior of wind turbines which experience fatigue loading at a frequency of 1 Hz.

Finally, there are the issues of potential fatigue limits in the R=2 and R=0.1 graphs. It is uncertain whether these

limits may exist, and the subject is definitely a potential area for future research.

REFERENCES

REFERENCES

1. Committee on Assessment of Research Needs for Wind Turbine Rotor Materials Technology, "*Assessment of Research Needs for Wind Turbine Rotor Materials Technology*", National Academy Press, Washington, D.C., 1991.

2. James, G., "Vibration Analysis and Suppression: Modal Validation and System Identification", Meeting on Department of Energy Wind Technology Program, Denver, October, 1993.

3. Creed, R.F., "High Cycle Tensile Fatigue of Unidirectional Fiberglass Composite Tested at High Frequency", Montana State University Masters Thesis, Chemical Engineering Department, 1993.

4. Reifsnider, K.L., *Fatigue of Composite Materials*, Elsevier Science Publishers B.V., Chapters 2-4, 1990.

5. Dew-Hughes, D. and Way, J.L., "Fatigue of Fibre-Reinforced Plastics: A Review", *Composites*, 1973, p. 167-173.

6. Dharan, C.K.H., "Fatigue Failure in Graphite Fibre and Glass Fibre-Polymer Composites", *Journal of Materials Science*, Vol. 10, 1975, pp. 1665-1670.

7. Mandell, J.F., "Fatigue Behaviour of Fibre-Resin Composites", in *Developments in Reinforced Plastics-2*, G. Pritchard, Ed., Applied Science Publishers, 1982, pp. 67-107.

8. Salkind, M.J., "Fatigue of Composites", in *Composite Materials: Testing and Design (Second Conference), ASTM STP 497*, American Society for Testing and Materials, 1972, pp. 143-169.

9. Broutman, L.J., "Failure Mechanisms for filament reinforced plastics", *Modern Plastics*, Vol. 42, 1965, pp. 143-216.

REFERENCES - Continued

10. Owen, M.J. and Dukes, R., "Failure of Glass-Reinforced Plastics Under Single and Repeated Loading", *Journal of Strain Analysis*, Vol. 2, 1967, pp. 272-279.

11. Broutman, L.J. and Sahu, S., "Progressive Damage of a Glass Reinforced Plastic During Fatigue", 24th Annual Technical Conference, Reinforced Plastics/Composites Division, SPI, 1969, Paper 11-D.

12. Tanimoto, T. and Amijima, S., "Progressive Nature of Fatigue Damage of Glass Fiber Reinforced Plastics", *Journal of Composite Materials*, Vol. 9, 1975, pp. 380-390.

13. Dharan, C.K.H., "Fatigue Failure Mechanisms in a Unidirectionally Reinforced Composite Material", in *Fatigue of Composite Materials, ASTM STP 569*, American Society for Testing and Materials, 1975, pp. 171-188.

14. Greszczuk, L.B., "Compressive Strength and Failure Modes of Unidirectional Composites", in *Analysis of the Test Methods for High Modulus Fibers and Composites, ASTM STP 521*, American Society for Testing and Materials, 1973, pp. 192-217.

15. Rosen, B.W. "Mechanics of Composite Strengthening", in *Fiber Composite Materials*, American Society for Metals, 1965, pp. 58-75.

16. Hahn, H.T. and Williams, J.G., "Compression Failure Mechanisms in Unidirectional Composites", in *Composite Materials: Testing and Design (Seventh Conference), ASTM STP 893*, J.M. Whitney, Ed., American Society for Testing and Materials, Philadelphia, 1986, pp. 115-139.

17. Rosenfeld, M.S. and Huang, S.L., "Fatigue Characteristics of Graphite/Epoxy Laminates under Compression Loading", *Journal of Aircraft*, Vol. 15, pp. 264-268.

18. Ratwani, M.M. and Kan, H.P., "Compression Fatigue Analysis of Fiber Composites", *Journal of Aircraft*, Vol. 18, no. 6, pp. 458-462.

19. Rotem, A. and Nelson, H.G., "Failure of a Laminated Composite Under Tension-Compression Fatigue Loading", *Composites Science and Technology*, 36(1989), pp. 45-62.

REFERENCES - Continued

20. Schoeppner, G.A. and Sierakowski, R.L., "A Review of Compression Test Methods for Organic Matrix Composites", *Journal of Composites Technology & Research*, JCTRER, Vol. 12, 1990, pp. 3-12.

21. Adams, D.F. and Odom, E.M., "Influence of Test Fixture Configuration on the Measured Compressive Strength of a Composite Material", *Journal of Composites Technology & Research*, JCTRER, Vol. 13, 1991, pp. 36-40.

22. Wung, E.C.J. and Chatterjee, S.N., "On the Failure Mechanisms in Laminate Compression Specimens and the Measurement of Strengths", *Journal of Composite Materials*, Vol. 26, 1992, pp. 1885-1914.

23. Berg, J.S. and Adams, D.F., "An Evaluation of Composite Material Compression Test Methods", *Journal of Composites Technology & Research*, Vol. 11, 1989, pp. 41-46.

24. Dally, J.W. and Broutman, L.J., "Frequency Effects on the Fatigue of Glass Reinforced Plastics", *Journal of Composite Materials*, Vol. 1, 1967, p.424-443.

25. Broutman, L.J. and Gaggar, S.K., "Fatigue Behavior of Epoxy and Polyester Resins", *International Journal of Polymeric Materials*, Vol. 1, 1972, pp. 295-316.

26. Cessna, L.C., Levens, J.A. and Thomson, J.B., "Flexural Fatigue of Glass-Reinforced Thermoplastics", *Polymer Engineering and Science*, Vol. 9, 1969, pp. 339-349.

27. Stinchcomb, W.W., Reifsnider, K.L., Marcus, L.A. and Williams, R.S., "Effects of Cyclic Frequency on the Mechanical Properties of Composite Materials", AFOSR-TR-73-1907, VPI, July 1973.

28. Mandell, J.F. and Meier, U., "Effects of Stress Ratio, Frequency, and Loading Time on the Tensile Fatigue of Glass-Reinforced Epoxy", in *Long-Term Behavior of Composites, ASTM STP 813*, T.K. O'Brien, Ed., American Society for Testing and Materials, Philadelphia, 1983, pp. 55-77.

REFERENCES – Continued

29. Saff, C.R., "Effect of Load Frequency and Lay-Up on Fatigue Life of Composites", in *Long-Term Behavior of Composites, ASTM STP 813*, T.K. O'Brien, Ed., American Society for Testing and Materials, Philadelphia, 1983, pp. 78-91.

30. Mandell, J.F., "Fatigue Behavior of Short Fiber Composite Materials", in *Fatigue of Composite Materials*, K.L. Reifsnider, Ed., Elsevier Science Publishers B.V., 1990, pp. 231-337.

31. Mandell, J.F., Creed, R.F., Pan, Q., Combs, D.W., Shrinivas, M., "Fatigue of Fiberglass Generic Materials and Substructures", The Energy-Sources Technology Conference, New Orleans, January, 1994, pp. 207-213.

32. Hedley, C., "Mold Filling Parameters of Resin Transfer Molding of Composites", Montana State University Masters Thesis, Chemical Engineering Department, 1994.

33. Mandell, J.F. and Tsai, J.Y., "Effects of Porosity on Delamination of Resin-Matrix Composites", WRDC-TR-89-3032, Wright Research Development Center, April, 1990.

34. Ryder, J.T. and Walker, E.K., in *Fatigue of Filamentary Composite Materials*, K.L. Reifsnider and K.N. Lauraitis, Eds., ASTM STP 636, 1977, pp. 3-26.

35. Conner, J.D., Mandell, J.F., McGarry, F.J., "Compressive Fatigue in Glass and Graphite Reinforced Composites", 34th Annual Conference Reinforced Plastics/Composites, Society of the Plastics Industry, January 1979, New Orleans, Paper 4-A.

36. Mandell, J.F., Reed, R.M., Samborsky, D.D., Pan, Q., "Fatigue Performance of Wind Turbine Blade Composite Materials", 16th Annual Energy-Sources Technology Conference and Exhibition, American Society of Mechanical Engineers, January 1993, Houston, Vol. 14, pp.191-198.

37. Han, K.S., "Compressive Fatigue Behaviour of a Glass Fibre-Reinforced Polyester Composite at 300 K and 77 K", *Composites*, Vol. 14, 1983, pp. 145-150.

REFERENCES - Continued

38. Portanova, M.A., Poe, C.C., Whitcomb, J.D., "Open Hole and Postimpact Compressive Fatigue of Stitched and Unstitched Carbon-Epoxy Composites", in *Composite Materials: Testing and Design (Tenth Volume), ASTM STP 1120*, G.C. Grimes, Ed., American Society for Testing and Materials, Philadelphia, 1992, pp. 37-53.

39. Combs, D., Montana State University Masters Thesis, Mechanical Engineering Department, to be published.

40. Ten Have, A.A., "Wisper and Wisperx: A Summary Paper Describing Their Backgrounds, Derivation and Statistics", 16th Annual Energy-Sources Technology Conference and Exhibition, Houston, January, 1993, pp. 169-178.

41. *Engineering Materials Handbook*, ASM International, 1987, Volume 1, p.144.

42. Hull, D., *An Introduction to Composite Materials*, Cambridge University Press, 1981, pp. 154-173.

APPENDIX

GRIP DESIGN

In order for valid, reproducible compression testing to be accomplished in this project, it was necessary to utilize different grips from the ones employed earlier in high frequency tensile testing (Figure 44). The design finally

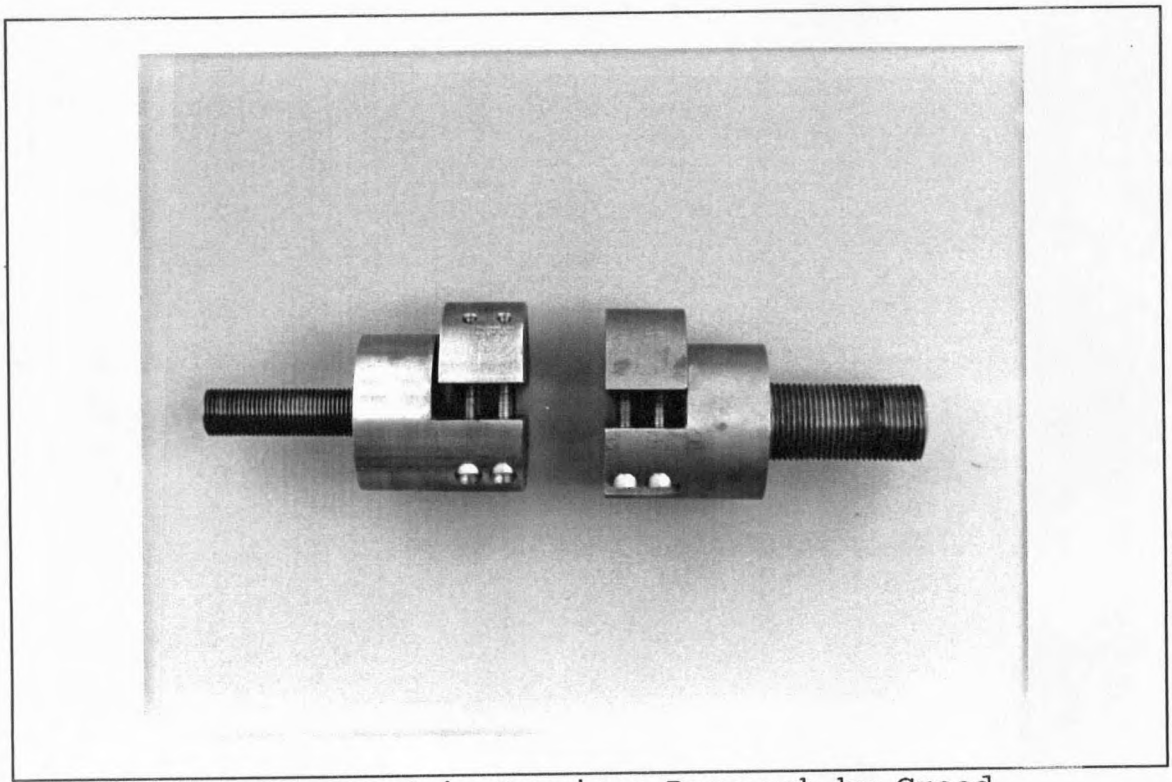


Figure 44. Grips Used in Previous Research by Creed.

chosen is illustrated in Figures 45 and 46. It provided even gripping force across the entire tab face, and was able to accommodate a wide variety of specimen thicknesses while

ensuring that the specimen was centered underneath the load applicator. These were testing requirements that the previous grips could not accomplish. Modifications were made to allow the grips to be used for compression testing. Four screws were incorporated into the outer shell to force the jaws together when tightened. This was necessary because compressive loads would act to force the jaws apart since the grips were originally designed to work only in tension. The screws were tightened to approximately 30 inch-pounds of torque during tests. The outer shell was composed of steel hardened to Rockwell C40, while the jaws were steel hardened to Rockwell C60. The jaws were also knurled, creating jaw faces that were able to solidly grip specimens by digging into the tabs.

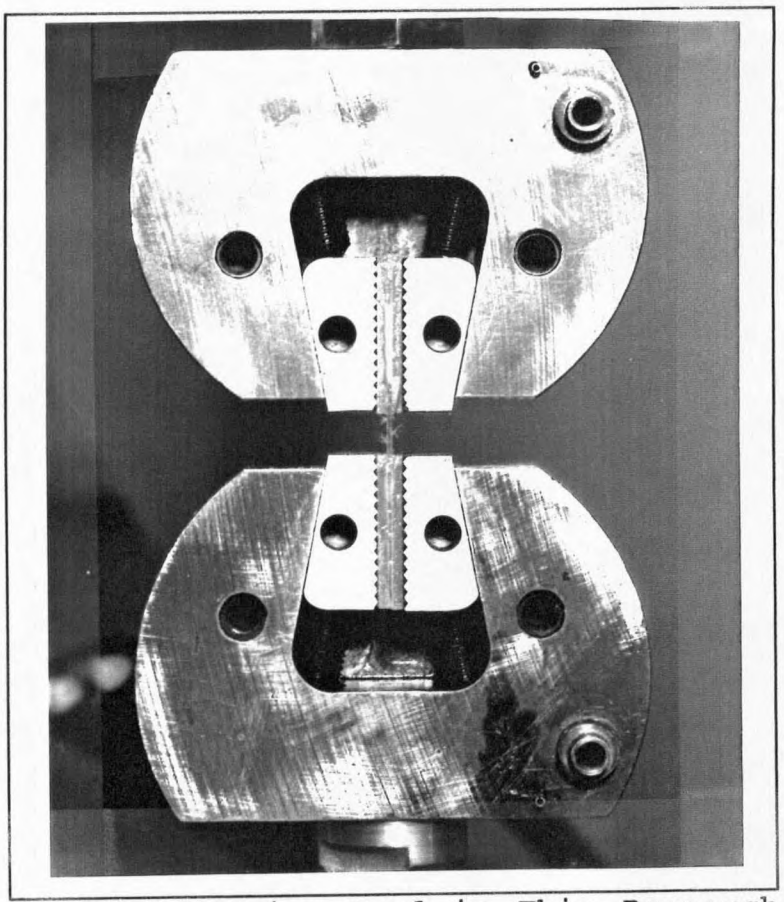


Figure 45. Grips Used in This Research with Specimen Running.

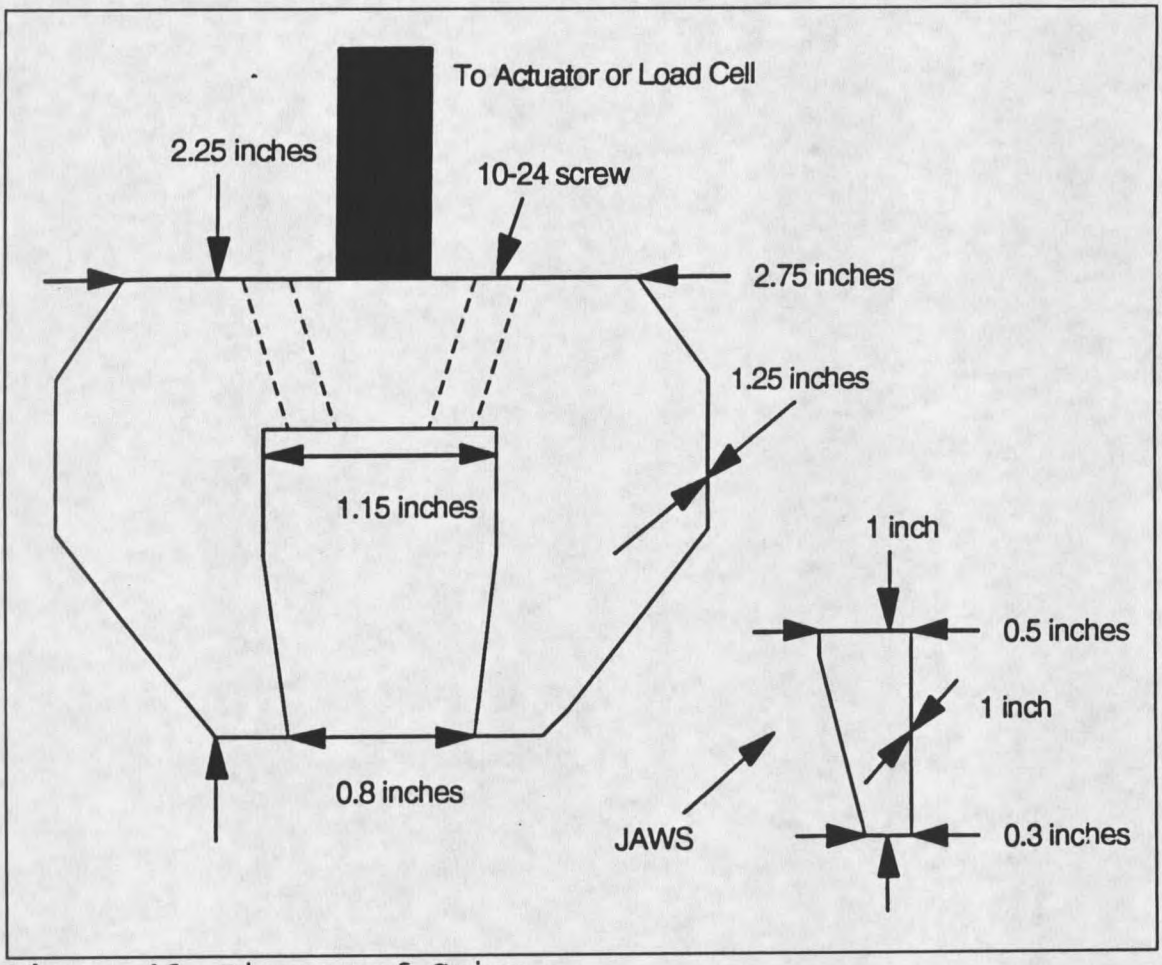


Figure 46. Diagram of Grips.

MONTANA STATE UNIVERSITY LIBRARIES
3 1762 10220069 6